NASA CR-117349

NATIONAL AERONAUTICS AND SPACE ADMINISTRATION

Technical Report 32-1519

Lightweight Solar Panel Development

Walter A. Hasbach

JET PROPULSION LABORATORY
CALIFORNIA INSTITUTE OF TECHNOLOGY
PASADENA, CALIFORNIA

March 15, 1971

NATIONAL AERONAUTICS AND SPACE ADMINISTRATION

Technical Report 32-1519

Lightweight Solar Panel Development

Walter A. Hasbach

JET PROPULSION LABORATORY
CALIFORNIA INSTITUTE OF TECHNOLOGY
PASADENA, CALIFORNIA

March 15, 1971

Prepared Under Contract No. NAS 7-100
National Aeronautics and Space Administration

Preface

The work described in this report was performed by the Space Division of the Boeing Company, under the cognizance of the Guidance and Control Division of the Jet Propulsion Laboratory.

Contents

Contents (contd)

Tables

Figures

Abstract

This report describes the work performed by the Boeing Co., Aerospace Group, Space Division, Seattle, Washington, between July 1, 1969, and July 1970, on the Lightweight Solar Panel Development Program under Jet Propulsion Laboratory Contract 952571. The report contains technical information concerning the preliminary design, analysis, test article design, fabrication, and test of a lightweight solar panel made of a built-up beryllium structure with an active cell area of 29 ft.^{2} Evaluations are presented of the results of the modal survey, reverberant acoustic, random vibration, sinusoidal vibration, static load, thermal–vacuum–shock, substrate frequency, and power output tests.

Lightweight Solar Panel Development

I. Introduction

The purpose of the Lightweight Solar Panel Development Program was to develop a solar panel, using the technology developed in the 50-kW Large Area Solar Array (LASA) Program,* that would satisfy the requirements for a smaller, 1-kW solar array with a substantial weight saving over conventional designs. The primary objective was to develop a lightweight solar panel having a power-to-weight capability of 20 W/lb that would meet the type approval requirements of a solar array for a hypothetical Mars mission within a time period needed to support a 1973 Mars flight. Secondary objectives were to (1) evaluate the array's capability to support added equipment, such as antennas, attitude control jets, and sun sensors, (2) evaluate the static and dynamic characteristics of the lightweight solar panel, (3) establish the thermal–vacuum and thermal shock capabilities of the lightweight solar panel, and (4) obtain parametric data and operating characteristics of zener diodes installed on the lightweight solar panel.

To establish a baseline for the panel design, it was determined that the panel would be as nearly interchangeable with the *Viking* class orbiter solar panels as could be determined at the time of design (Fig. 1). The solar panel would be tested to type approval levels specified for *Mariner* 1969 and modified as necessary to be compatible with the estimated *Viking* requirements.

The work was accomplished by the Boeing Co., Aerospace Group, Space Division, Seattle, Washington, under NASA/JPL Contract No. 952571, entitled "Lightweight Solar Panel Development." The contract period was from July 1, 1969, to July 1970.

*NASA/JPL Contract No. 951653, dated 1967.

II. Summary

Work on this contract has demonstrated that the technology developed on the Large Area Solar Array Program can be used to produce smaller, lightweight solar panels of about 1-kW capacity and with a power density of 20 W/lb. A configuration study was conducted to evaluate the effects of mounting additional equipment such as a 10-lb relay antenna, 2-lb sun sensors, 2-lb maneuver antenna, and 2.8-lb attitude control jets on the dark side of the solar panel. Results of these studies show only minor penalties in weight and thermal-electrical performance. Approximately 1.5 W of electrical energy is lost owing to equipment thermal effects, and the re-

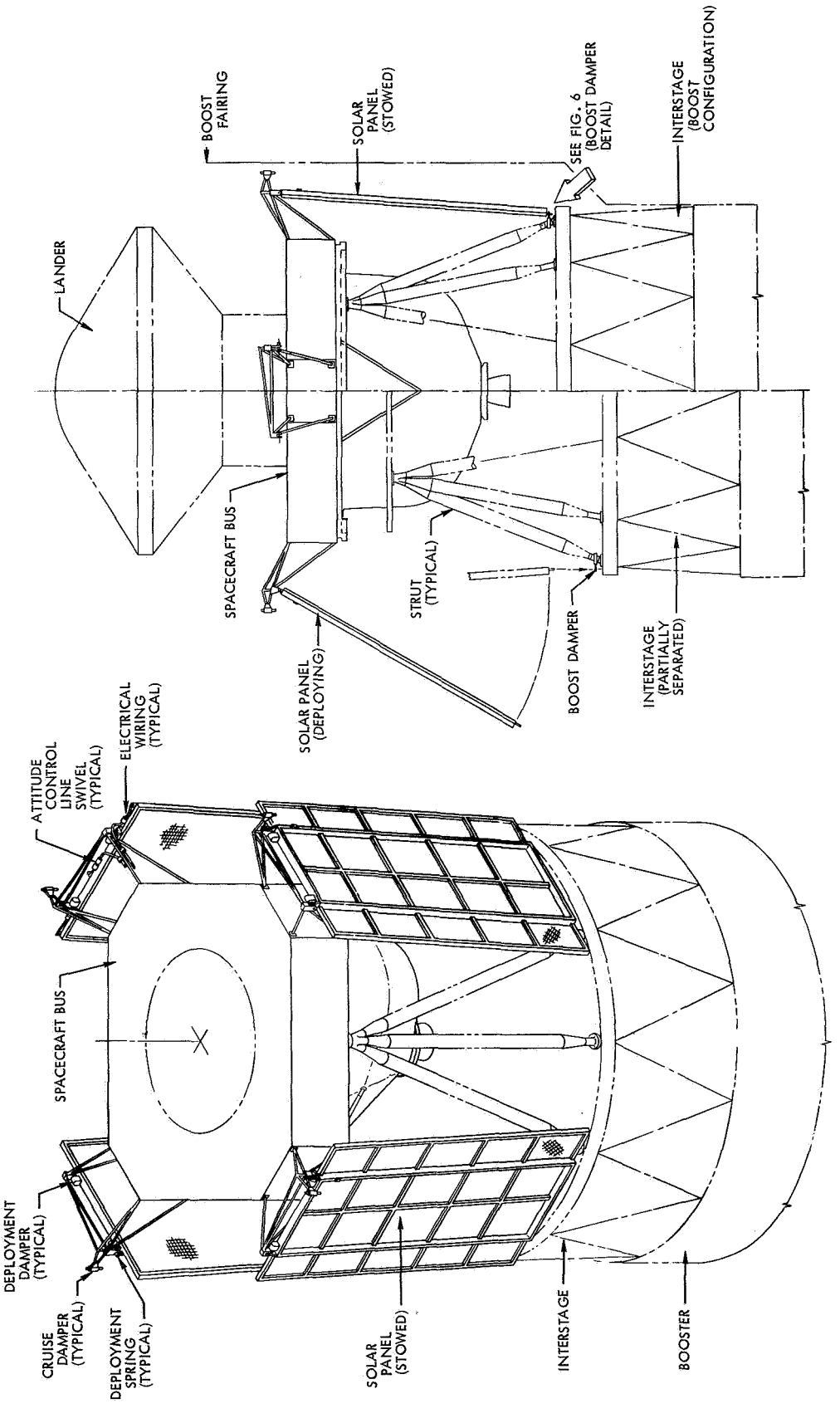

Fig. 1. Lightweight solar panel installation

quired structure to support the additional equipment results in a decrease in power density of 0.7 W/lb.

The lightweight solar panel fabricated and tested under this contract was 88.60 in. long and 51.00 in. wide. It was assembled with 0.008-in.-thick solar cells and had 0.003-in.-thick cover glass. The resulting power-to-weight ratios, excluding mechanisms and added equipment, are 20.6 W/lb without zener diodes and 17.0 W/lb with 5 zener diodes per module (12 modules per solar panel).

Test results were, in general, within those limits predicted during the design study phase. In the modal survey, the mode shapes agreed with those calculated. Frequencies were somewhat lower than expected; for example, 12.2 Hz was measured vs 17.0 Hz calculated for the first torsion mode. Accelerations and stresses measured during acoustic tests were within acceptable limits (3-sigma acceleration, 900 g peak, 305 g rms). Random vibration stress and acceleration levels were low, as expected, and were not excessive in the area of concern near the attitude control jets. Acceleration levels on the substrate were 14.6 g rms and at the simulated 2.8-lb attitude control jets were 6.1 g rms. The highest stress was located at the main spar and was measured at 1100 psi. Sinusoidal vibration stress and acceleration were below damage levels. Acceleration of the substrate was 12.5 g peak, and the structure was 5g peak, except for a peak of 15 g on the longitudinal intercostal. The highest stress was measured at 3,250 psi (vs 10,900 psi for zero margin of safety). The static load test to determine terminal stiffness indicated deflections greater than predicted by 50% in torsion and 20% in bending, but was as expected from the modal test results. The highest stress was measured to be 7400 psi on the spar cap in bending vs 6550 psi calculated.

The successful conclusion of this program demonstrates technology readiness of this design for use on deep space missions requiring lightweight solar arrays. Among the design features are its high power-to-weight ratio, structural stiffness, desirable thermal characteristics (i.e., balanced thermal coefficients of linear expansion and minimum stable temperature), and its ease of manufacture.

III. General Design Description

Various solar panel designs were made and evaluated to study the impact of mounting additional equipment on the dark side of the solar panel. The effects of these appendages on weight and power performance are shown in Fig. 2. Noted in this figure is the evolution from the initial design, at the contract start, to that configuration which was ultimately tested and designated as configuration III. A comparison of the results of this study shows only minor penalties in weight and thermal–electrical performance when additional equipment is supported by the panel. Following the analysis of the various designs, a decision was made to proceed with a test panel omitting the relay antenna and maneuver antenna; the sun sensor was located on the longitudinal center line. Other equipment attached to the solar panel, as tested, is shown in Fig. 3; this equipment includes electrical connections, buses, diodes, the simulated attitude control subsystem, simulated sun sensors, and mechanical elements such as the hinges and boost damper pins.

The basic panel structural design consists of a pretensioned fiberglass tape substrate sandwiched between sun-side and dark-side bonded beryllium frames as shown in Fig. 4. The dark-side frame includes outboard spars and edge members which form the perimeter of the frame, two longitudinal main spars, a center longitudinal intercostal, and lateral intercostals. The sun-side frame consists of perimeter members only. All primary structural adhesive bonding, including the beryllium spars and intercostals and the final frame-to-substrate-to-frame bond, is accomplished with a modified epoxy film supported with dacron fibers. Titanium is used at concentrated load points and joints between structural components where it is more suitable. Electrical-discharge-machined titanium fittings are used for the spacecraft attachment hinges and the tip latch fittings, which support the tip latch pins.

Table 1 presents actual weight data for components of the test panel. Where weight tests were not made, the detailed weights are noted as being estimated. The total of this column varied from the measured weight of the completed test panel by 0.33 lb. The most probable source of this variance is in the weights of thermal control coatings, wires, and miscellaneous parts, which are generally of an unestablished accuracy. The center-of-gravity location was determined by measurement of the test panel shown in Fig. 3 as follows:

(1) Longitudinal datum: 53.4 in. from the hinge centerline.

(2) Lateral datum: 24.9 in. from the outer edge of the outboard spar adjacent to modules 1 through 8.

CONFIGURATION I

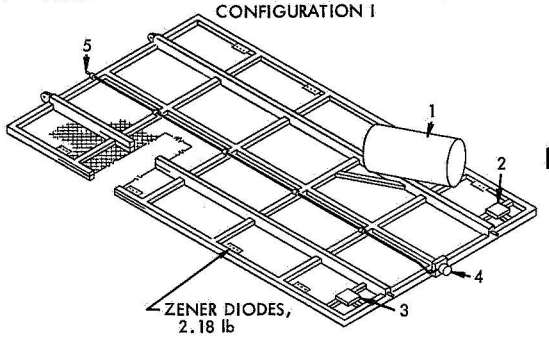

SIMULATED ADDITIONAL EQUIPMENT

1 RELAY ANTENNA, 15 lb
2 SUN SENSOR, 2 lb
3 MANEUVER ANTENNA, 2 lb
4 ATTITUDE CONTROL JET, 1.4 lb
5 ATTITUDE CONTROL LINE, 0.55 lb

BASELINE CONFIGURATION II

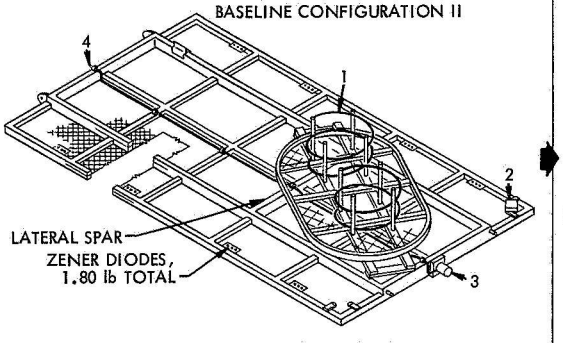

SIMULATED ADDITIONAL EQUIPMENT

1 RELAY ANTENNA, 10 lb
2 SUN SENSOR, 2 lb
3 ATTITUDE CONTROL, 2.8 lb
4 ATTITUDE CONTROL LINE, 0.88 lb

TEST PANEL CONFIGURATION III

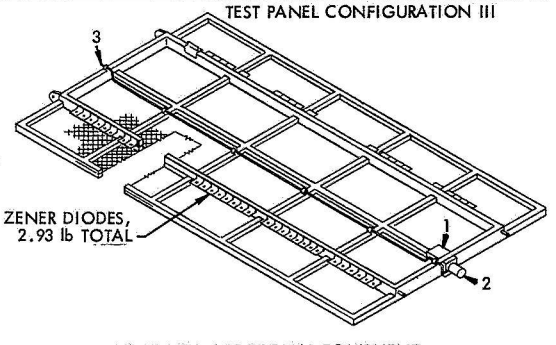

SIMULATED ADDITIONAL EQUIPMENT

1 SUN SENSOR, 2 lb
2 ATTITUDE CONTROL JET, 2.8 lb
3 ATTITUDE CONTROL LINE, 0.88 lb

ALTERNATE CONFIGURATION IV

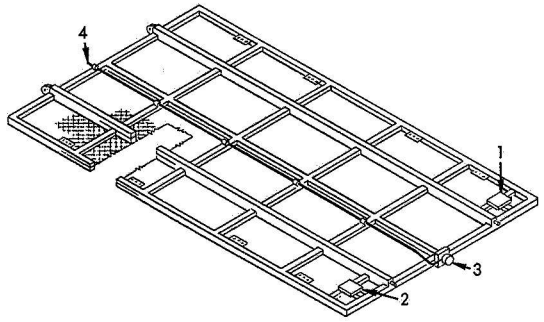

SIMULATED ADDITIONAL EQUIPMENT

1 SUN SENSOR, 2 lb
2 MANEUVER ANTENNA, 2 lb
3 ATTITUDE CONTROL JET, 1.4 lb
4 ATTITUDE CONTROL LINE, 0.88 lb

ALTERNATE A CONFIGURATION V

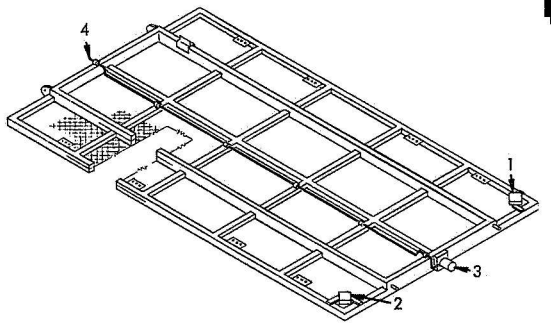

SIMULATED ADDITIONAL EQUIPMENT

1 SUN SENSOR, 2 lb
2 MANEUVER ANTENNA, 2 lb
3 ATTITUDE CONTROL JET, 2.8 lb
4 ATTITUDE CONTROL LINE, 0.88 lb

RESULTS OF CONFIGURATION REVIEW
(BASED ON A FOUR-PANEL ARRAY
INSTALLED ON A SPACECRAFT)

CHARACTERISTIC	BASELINE CONFIGURATION II	CONFIGURATION IV	CONFIGURATION V
INTERCHANGEABILITY	YES	YES	NO
POWER LOSS AT MARS DUE TO EQUIPMENT THERMAL EFFECT	2.0W	0.5W	2.0W
SOLAR ARRAY WEIGHT, lb			
CELL STACK AND STRUCTURE	56.52	54.84	54.36
MECHANISMS	10.40	10.40	10.40
EXTRANEOUS EQUIPMENT	44.88	31.92	44.88
TOTAL	111.80	97.16	109.64
POWER-TO-WEIGHT RATIO AT 10 W/ft^2 BASED ON CELL STACK AND STRUCTURE WEIGHT ONLY	20.5 W/lb	21.2 W/lb	21.3 W/lb

Fig. 2. Solar panel design evolution

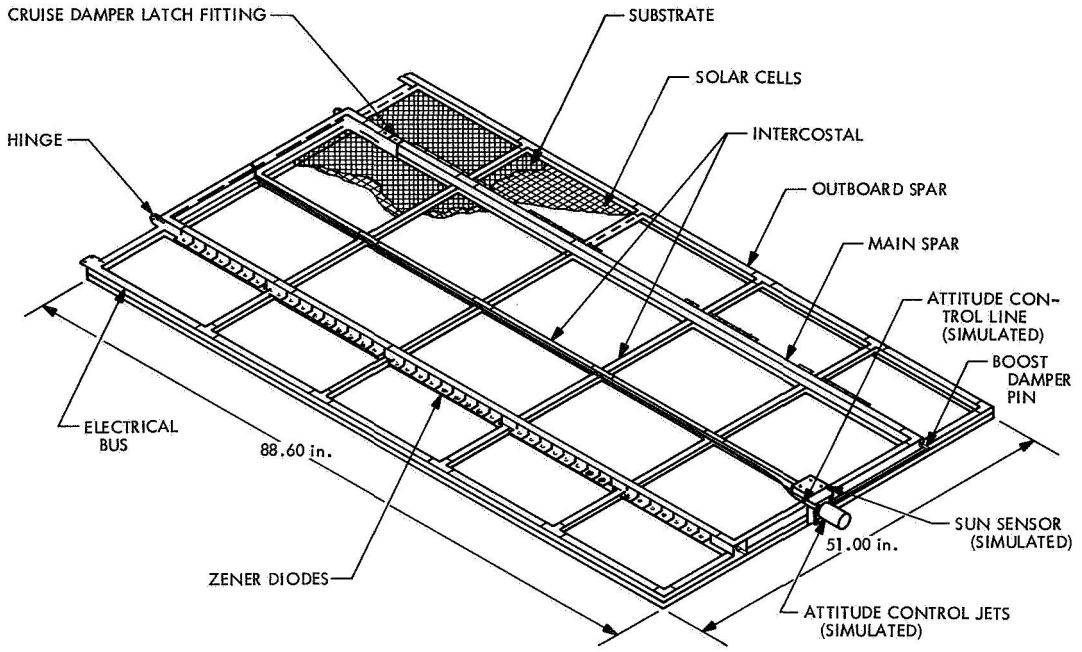

Fig. 3. Test panel configuration III

This includes all dummy masses. The center of gravity is 0.6 in. off the longitudinal centerline (because of the off-center distribution of the zener diodes) and nearer the outboard end of the panel.

The following mass-simulated equipment is mounted to the structure:

(1) Cruise latch. No attempt has been made to simulate the actual latch hardware except for the weight allowance and weight distribution on the panel structure.

(2) Sun sensor. This item is simulated by a block of steel. It is attached to the test panel by bolting to titanium clips bonded to the panel structure.

(3) Attitude control equipment. The weight of the dual attitude control jets is simulated by a steel cylinder with mounting flanges. The 2.8-lb cylinder is shaped to provide the assumed correct center-of-gravity distance from the titanium mounting bracket bonded to the panel structure. The attitude control tubing is simulated by a stainless steel tube clamped at several locations along the center longitudinal intercostal. There was no attempt to install electrical control circuit simulation or tubing swivel joint simulation at the deployment centerline.

Deployment equipment design has been performed in sufficient depth to support the analysis and selection of the deployment equipment shown in Fig. 5. This equipment includes:

(1) Deployment spring.

(2) Rotary dampers.

(3) Roller.

(4) Bearings.

The first three items were carried through the design phase only and were not included on the test panel. The flight installation of the boost dampers is shown in Fig. 6. Dampers of the *Mariner* Venus 67 type were used in this installation for the vibration tests of the panel.

IV. Solar Panel Electrical Design

An objective of the solar panel development was to provide electrical power output of 20 W/lb of panel weight at 1 au and 55°C. Based on 10 W/ft^2 and a total solar array cell area of 116 ft,^{2} the predicted output for the flight configuration is 1160 W. Final predicted weight of a four-panel array is 56.28 lb without zener diodes, 68.44 lb with five zener diodes per module and 63.53 lb with three zener diodes per module. The resulting power-to-weight ratios, excluding mechanisms and added equipment are 20.6 W/lb without zener diodes, 17.0 W/lb with five zener diodes per module, and

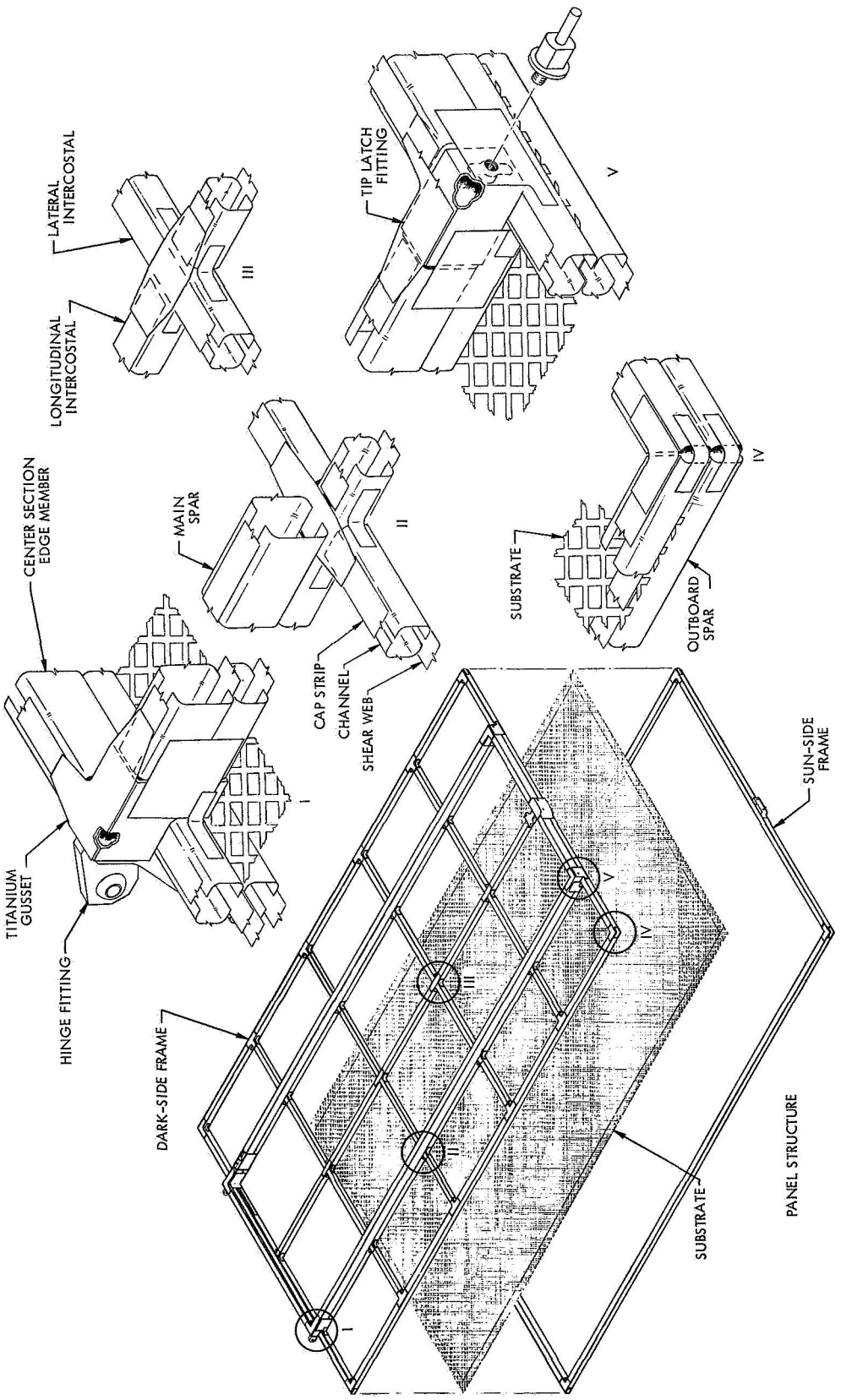

Fig. 4. Test panel structural assembly

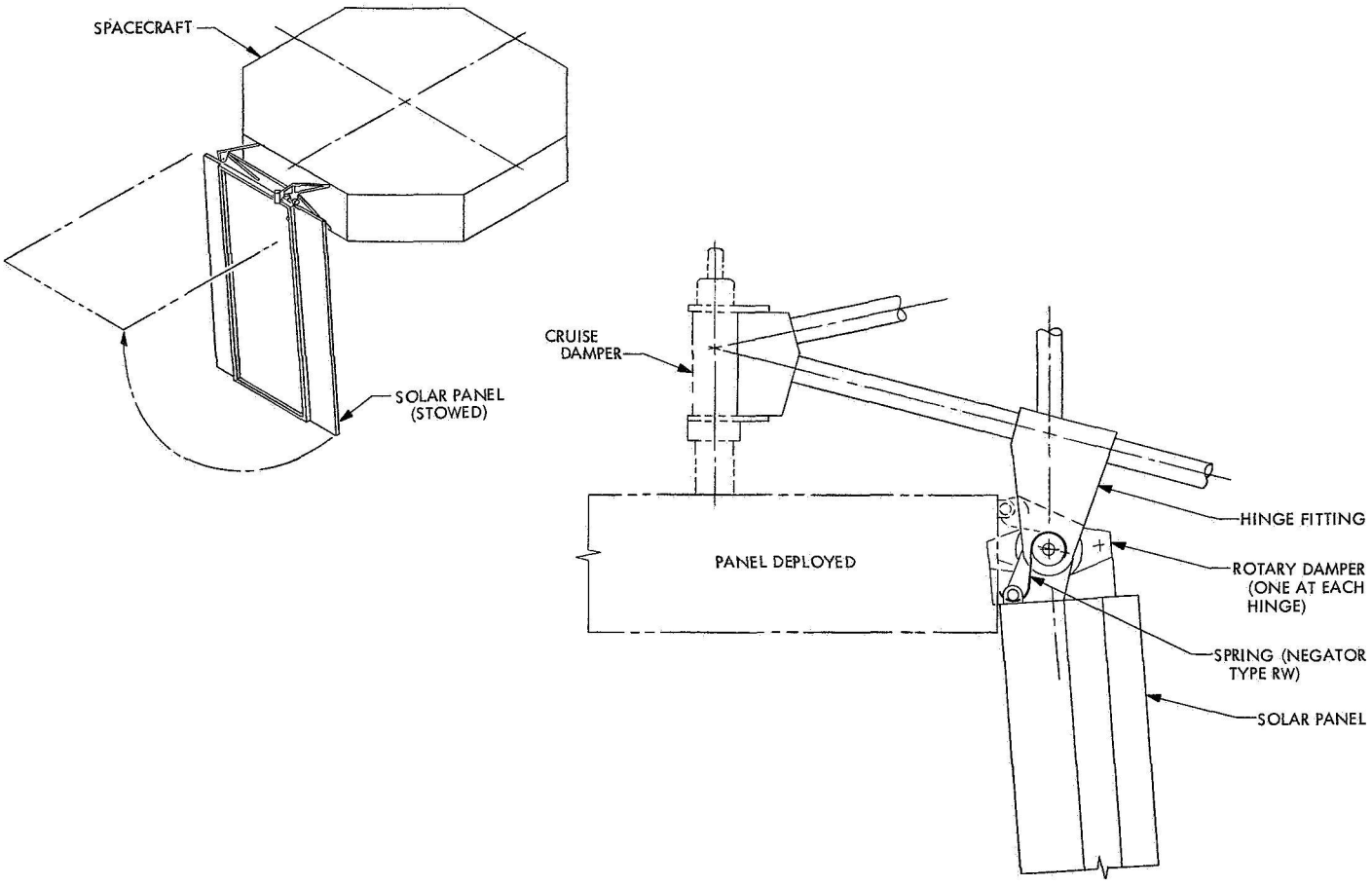

Fig. 5. Deployment equipment

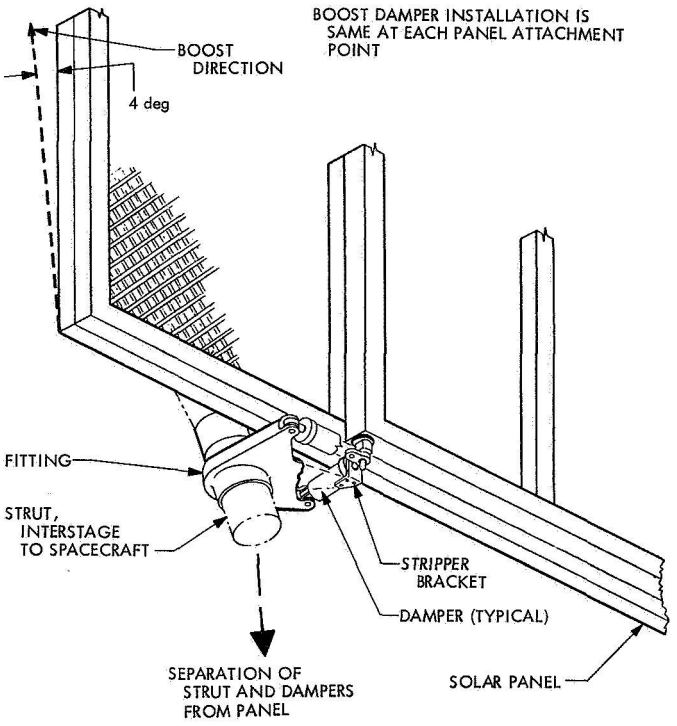

Fig. 6. Boost damper detail

18.2 W/lb with three zener diodes per module. In the flight configuration, each module is electrically connected to five 10-V zener diodes connected in series to limit the module output to 50 V.

The electrical design includes 12 solar cell modules per panel arranged and connected as shown in Fig. 7. The test panel electrical installation and details of components are shown in Fig. 8. The solar cell coverglass combinations are bonded to the panel substrate in the form of submodules. Each submodule is 6 or 7 cells wide by 20 or 40 cells long. The cell groups of 6 or 7 cells in parallel are interconnected by expanded silver mesh strips which contact the adjacent cell group to provide a series connection of 80-cell groups for each module. Each submodule is bonded to the substrate using RTV-40, which serves as both an adhesive and a thermal control coating on the dark side of the cells.

The test panel configuration has three 16-V zener diodes for modules 7 and 9, four 12-V diodes for modules 5 and 11, and five 10-V diodes for modules 3 and 10. The remaining diodes are mass-simulated to provide weight equivalent to five diodes for each of the 12 modules. Electrical power buses are integrated with the outboard spars. Bus assemblies are made from alternate layers of Kapton film (1 mil thick), thermoplastic polyester resin (1 mil thick), and copper strip (5 mils thick). The film is wider than the copper so that the conductors are completely encapsulated. The assembly is attached to the structure with RTV-630, a silicone elastomer. Installation of inboard power terminals and bus construction are shown in Fig. 8.

Table 1. Test panel weight summary

Component	Preliminary weight estimate, lb	Actual weight, lb
Cell stack and buses (total)	(5.15)	(5.75)
Solar cells, 6480, 2 × 2 cm, 8 mil thick	2.49	2.49[a]
Coverglasses, 3-mil microsheet, 2 × 2 cm	0.91	1.02[a]
Cell adhesive	0.30	0.30[a]
Coverglass adhesive	0.12	0.12[a]
Solder and connectors	0.38	0.42[a]
Buses and terminals	0.45	0.60[b]
Thermal coating	0.50	0.80[b]
Panel structure (total)	(8.06)	(8.30)
Main spars	1.68	1.66
Outboard spars	1.56	1.40
End members	1.21	1.20
Lateral intercostals	0.76	0.70
Longitudinal intercostals	0.34	0.33
Substrate	0.46	0.46[a]
Clips, splices, gussets	0.68	0.75
Thermal coating	0.35	0.38[b]
Fittings	0.68	0.88
Miscellaneous	0.34	0.54[b]
Subtotal (structural and electrical)	(13.21)	(14.05)
Diode installation (total)	(2.93)	(3.05)
Zener diodes	2.45	2.45
Mounting strips	0.48	0.60
Attitude control (simulated)	(3.68)	(3.85)
Attitude control jets	2.80	2.83
Tubing installation	0.88	1.02[b]
Panel mechanisms	0.07	0.07
Sun sensor	(2.00)	(2.00)[b]
Total	21.89	23.02
Variance between predicted and measured (1.43%)		+0.33
Measured total		23.35

[a]LASA weight test data used.
[b]Estimated.

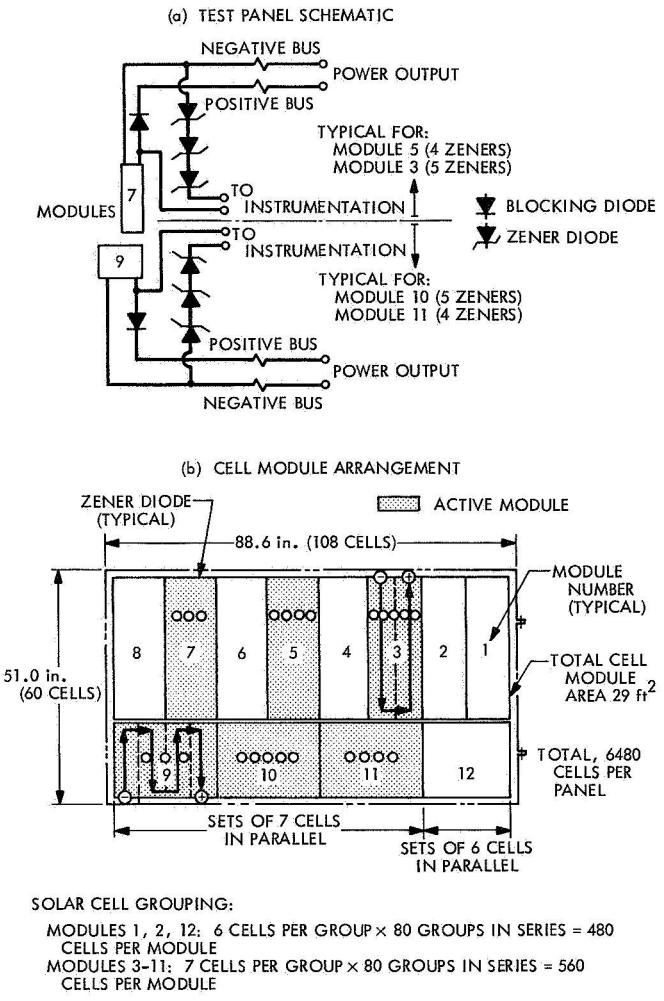

Fig. 7. Electrical design

The solar cell used in this analysis provides 0.0475 W at 140 mW/cm² intensity and 55°C temperature. A total of 6480 such cells per panel provides about 308 W with a gross cell module area of about 29 ft,² resulting in 10.6 W/ft.² The ratio of cell module area to gross panel area (29 to 31.4 ft²) is greater than 92%.

Twelve modules, each with 80-cell groups in series were used to obtain an optimum cell module and structure packaging arrangement. This arrangement provides 33.6 V near earth and 46.4 V near Mars. The application of zener diodes to overvoltage protection was analyzed. Two cases were considered: (1) a spacecraft emerging from behind Mars at 1.62 au after orbit occultation, and (2) near-earth maneuvers where the array may be off-sun for up to 90 min. The near-earth condition was found to be the most severe with the cell temperature as low as −198°C and a worst-condition module output of 42.5 W, without considering cell warmup characteristics. The wattages for three, four, and five zener diodes per module are:

Zener diodes per module	Watts per diode
3	14.1
4	10.6
5	8.5

With zener diodes rated at 50 W and a conservative rated-power-to-dissipated-power ratio of 4 to 1, each zener can accommodate up to 12.5 W. This indicates that either four 12-V zeners or five 10-V zeners per module would provide a conservative design. Because of the short cell warmup time provided by the open fiberglass tape substrate design, the voltage is above the maximum for only a short period of time, and the peak power per module that must be dissipated is more nearly 35 W, which allows the use of three zeners per module, with about 11.7 W being dissipated by each zener.

Normal operating temperature for a flight configuration panel is 45.5°C as compared to the 55°C design objective. In the area of sun sensor blockage of the cell dark side, the temperature is 71°C. This blockage results in a power loss of about ¼ W. The antenna blockage, analyzed for configuration II, resulted in a 1.5-W power loss.

V. Dynamic and Stress Analyses

During the preliminary design phase, the initial dynamic and stress analyses showed that panel weight could be minimized by panel design which met the static and frequency requirements and by provision of sufficient damping to control the dynamic stresses. The selected boost support condition allows tip motion by connection of the main spar tips to ground through the damper springs. The resulting pin-free mode exhibited a node near the CG of the 10-lb antenna, reducing its dynamic effect. When the antenna was removed, the dynamic and stress analyses were refined to include the revised weight and the minor structural changes which resulted in the test panel.

Solutions for the deflections and member loads due to static requirements and for the resonant mode shapes, frequencies, and dynamic loads for the normalized deflections were obtained with the Boeing ASTRA (Advanced Structural Analyzer) computer program. The

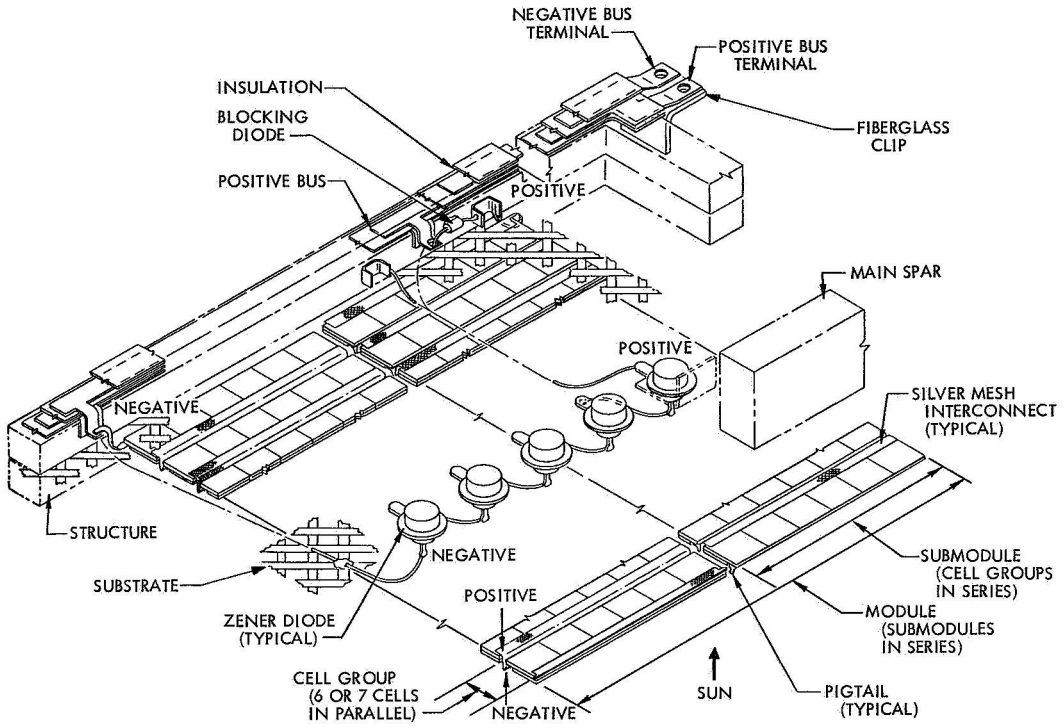

Fig. 8. Test panel electrical installation

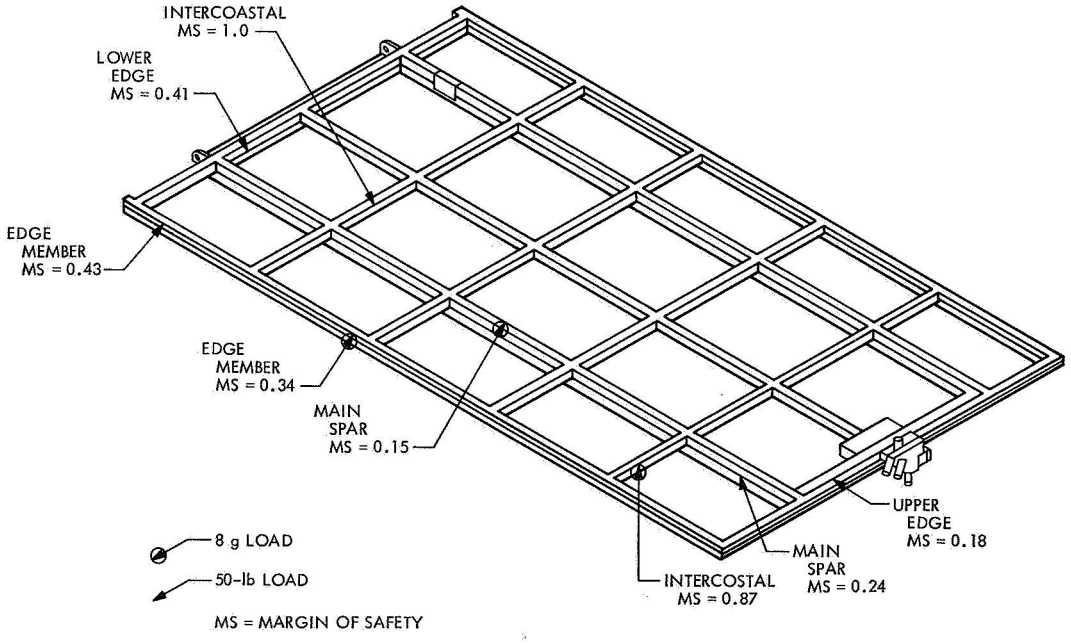

Fig. 9. Static stress margins

program is designed to analyze large complex structures using the direct stiffness matrix method (damping is not included). The program defines structural members by nodes. A node was assumed at each structural member intersection, at the center of each substrate bay, and at the mass-centers of the simulated sun sensor and attitude control jet.

The basic rectangular framework was idealized with beam elements between the nodes. Substrate bays were represented by an "overlay" of plate elements which provide only shear stiffness equivalent to that of the fiberglass diagonal tapes for in-plane vibrations. For out-of-plane vibrations, the substrate stiffness was represented by a pair of diagonal beams having only bending stiffness. Short, stiff beam elements were used for the damper fittings (outboard support points), for the hinge fittings, and for the supports required for the sun sensor and the guidance and control jet assembly.

Concentrated weights at the nodes represented the distributed weight. It was assumed that ½ the weight of each member ending at a node was effective at the node. For static loads, ¼ the weight of each substrate bay was assigned to the corner structural nodes. For in-plane (shear) dynamic analysis, the substrate weight was distributed to the corner nodes, similar to the static loads. For out-of-plane vibration, the early analyses assumed that the generalized mass for the fundamental substrate mode (¼ of the total substrate mass) was at the center of the substrate bay with the remaining ¾ distributed to the corners. Cross sections of the structural framework members were defined, and the structural stiffness characteristics of each member were defined in the computer input by the cross-section area, torsional stiffness, shear areas, and bending (stiffness) moment of inertias in two directions, and by elastic properties of the material.

The stiffness of the diagonal beams representing the substrate in out-of-plane bending was selected to result in a specified frequency when loaded with the generalized mass at the intersection of the beams. The analyses were made with the substrate nodes suppressed by an increase of beam stiffness by a factor of 10, which raised the lowest resonance to above 100 Hz. Early analyses, with the substrate modes included, showed a band of 20 closely spaced frequencies starting at 42.5 Hz, which effectively masked the structural modes in the region. Because the ASTRA program cannot include damping, the effect of the substrate modes on resonances within the 20-frequency band is exaggerated. To provide visibility for the basic structural modes, the unrealistic undamped response of the substrate was removed. This provided a close approximation of the resonant frequencies, and refinement could be made at a later date if necessary.

The output of the ASTRA program provided the complete loading (end load, shear, bending, and torsion) for each member for both the static and dynamic solutions with damping excluded. Stresses due to tape tension and to manufacturing straightness tolerances are combined with those from the external loads.

Member loads were calculated for a total load of 8 times the weight distributed to the nodes and for a 50-lb load applied to one outboard support. Stresses were then calculated for the two-load conditions without the 1-g load added; deflections were obtained for comparison with test measurements.

Margins of safety for the dynamic cases were calculated for selected percentages of the normalized amplitude to define the limiting amplitude for a positive margin of safety. This, in turn, defines the damping force required to limit the motions. All limit loads are multiplied by 1.25 to obtain the ultimate design load. Where appropriate, they are also multiplied by a 1.15 fitting factor.

Dynamic solutions for the resonant frequencies and mode shapes were also derived from the ASTRA computer program, as were the generalized inertia and stiffness matrices. Response calculations were originally made by use of a supplementary program which retrieved stored data from ASTRA tapes to yield the complex response of the normal modes (pin-free) coupled by the damper and driven by the inertia coupling between the excitation motion and the driven modes. Examination of the results showed that a simplified approach was possible. This approach utilized the pin-free normal modes with the panel tip connected to ground through the damper springs. The modal coupling due to the damping forces was neglected, and the driving inertial forces were hand-calculated. At resonance, the driving force is balanced by the damper force, conservatively assuming that the panel damping is small.

Stress analysis results are shown for the static load conditions in Fig. 9 and for the critical dynamic condi-

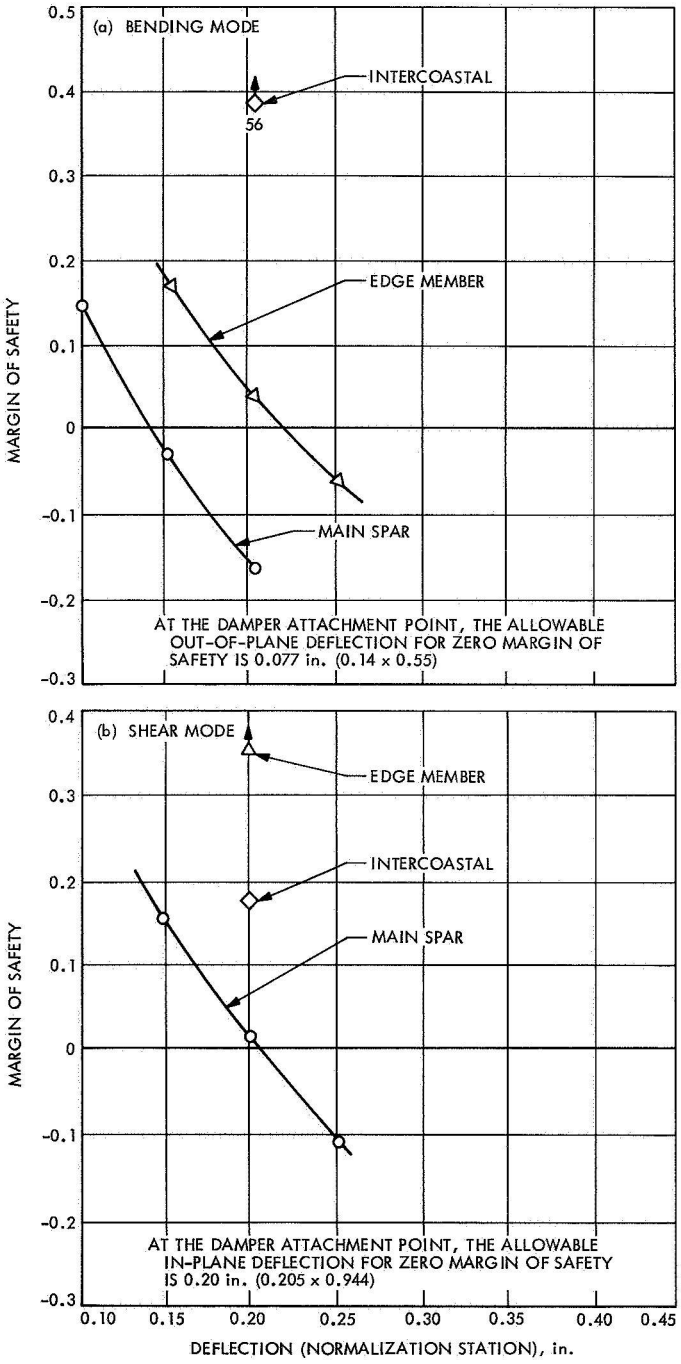

Fig. 10. Dynamic margins of safety vs deflection

tions in Fig. 10. These results reflect the preliminary estimated test panel weights given in Table 1. These detailed analyses resulted in the addition of doublers (i.e., structure reinforcement) which improved the margins of safety where required. The deflection shapes for the 8-g and 50-lb static load conditions are shown in Fig. 11.

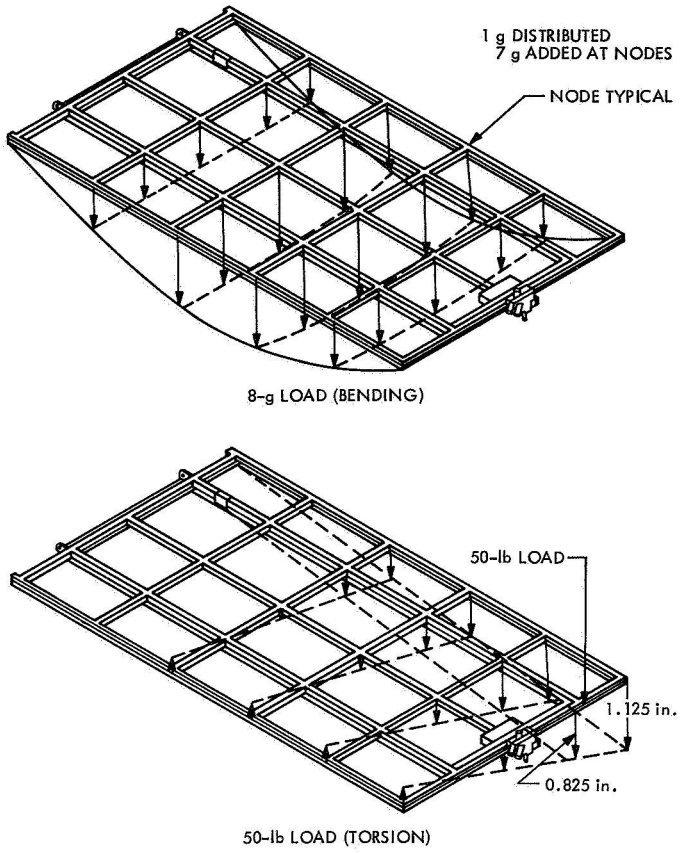

Fig. 11. Static deflection shapes

Dynamic analysis results for the resonant frequencies for four support configurations are tabulated in Table 2. These calculated values were obtained with the substrate frequencies increased by a factor of about 3 to provide visibility for the structural modes. The first configuration relates to the boost configuration and the sinusoidal sweep tests; the second, to the modal test. From the computer-calculated mode shapes and the excitation motions of translation (specified requirement) and hinge excitation (test requirement), the driving forces for each mode were calculated for a 1-*g* input. From these values the sinusoidal test levels were derived. The modal test setup introduced a rigid rotation mode at about 1 Hz, but did not affect the tabulated frequencies.

The third configuration tabulated (pin–pin) shows that the minimum calculated frequency exceeds the required (20 Hz) by a considerable margin. The minimum deployed configuration frequency, which was calculated using a *Mariner* Venus 67 cruise damper spring at a 7-in. arm, is 1.6 Hz. With a 6.5-in. arm and 0.7 critical damping, the frequency is 1.07 Hz, which is greater than the required minimum frequency of 1.0 Hz.

Table 2. Analysis results, resonant frequencies

Support condition	Rigid rotation	First torsion	Shear	First bending	Second torsion	Chord bending	Second bending
	Resonant frequencies, Hz						
Pin-free (35-lb/in.-springs in boost dampers)	7.9	19.2	28.5	34.3	68.6	80.9	103.3
Pin-free (modal survey)	–	17.0	27.5	33.9	67.9	80.9	103.0
Pin-pin	–	45.6	27.4	28.8	–	79.6	99.6
Deployed (530-lb/in.-springs in cruise damper)	1.61	17.2	27.5	34.5	–	–	–

VI. Panel Deployment Velocity Limitation

The approach which was selected provides a conservative approximation of the maximum panel deployment velocity. A more detailed analysis was not performed because a higher opening velocity limit would not significantly affect deployment mechanism requirements. For example, if the deployment velocity could be increased from 0.22 to 0.24 rad/s, two rotary dampers would still be required.

The assumptions used in this analysis are diagrammed in Fig. 12. The deploying panel is idealized as a single spar with 17.02 lb of the panel weight evenly distributed along the spar length. Torsional loads on the spar have been included in establishing the 960-in.-lb maximum spar bending moment. The 4.87 lb of tip-mounted equipment is assumed to be concentrated on the end of the spar, 80 in. from the hinge. Effect of the cruise damper latch is assumed to be included in the 530-lb/in. spring rate of the cruise damper spring. Damping coefficient of the cruise damper is assumed to be 80 lb/in./s. The value d, described in Fig. 12, has been neglected in the development of cruise damper force-deflection curves but is considered as part of the ratio of energy absorbed to absorption capability of both the panel and the cruise damper, which has been arbitrarily defined not to exceed a limit of 60%.

The approach used to establish the closing velocity limitation is shown in the following sketch and subsequent conditions:

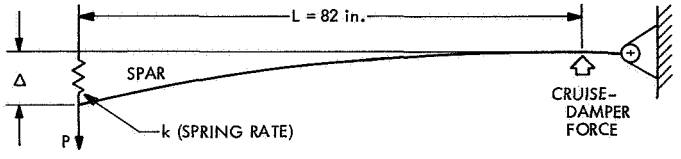

(1) Kinetic energy of a deploying panel is found by the formula $KE = (1/2)IO^2$, where I = 18.5 slug-ft² and O = angular velocity at latching.

(2) The energy absorbing capability of a panel spar is found as follows, for a maximum spar bending moment M = 960 in.-lb:

$P = M/L = 11.7$ lb

Δ = tip deflection = 0.75 in.

k= spar spring rate = P/Δ = 15.6 lb/in.

Potential energy = $(1/2)\ K\Delta^2$ = 4.36 in.-lb (maximum spar capability)

(3) The energy-absorbing capability of the cruise damper is found by integrating the force-deflection curves for the damper and the damper spring and adding these for each deployment velocity considered, as shown in Fig. 13. In developing these curves, the spar is assumed to be infinitely stiff in bending. Thus, for each small increment of time from first contact to the final position, the acceleration given by

$$\frac{\text{(initial velocity)} - \text{(final velocity)}}{\text{time interval}} =$$

the acceleration given by

$$\frac{\text{(cruise damper force) (6.5-in. moment arm)}}{18.5 \text{ slug-ft}^2}$$

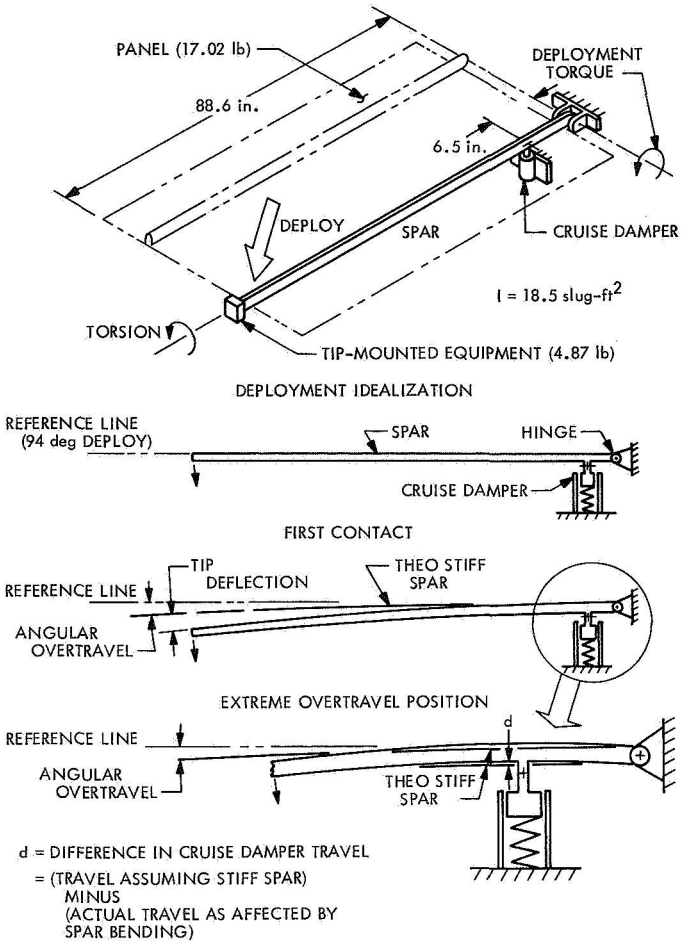

Fig. 12. Deployment analysis assumptions

DAMPER FORCE-DEFLECTION CURVE	AREA UNDER CURVE, in.-lb	SPRING FORCE-DEFLECTION CURVE	AREA UNDER CURVE, in.-lb	TOTAL AREA (ENERGY), in.-lb
1 , 0.30 rad/s	7.97	S_1	1.42	9.39
2 , 0.25 rad/s	5.02	S_2	0.98	6.00
3 , 0.22 rad/s	3.85	S_3	0.77	4.62
4 , 0.20 rad/s	3.39	S_4	0.63	4.02

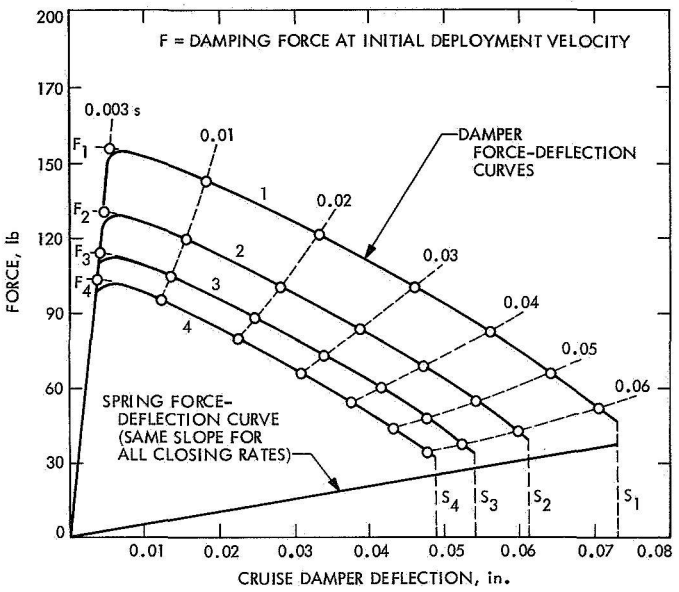

Fig. 13. Cruise damper force-deflection curves

A time limit of 0.063 s was used for the cruise damper force-deflection curves. This limit is based on a 4-Hz bending frequency of the spar and the assumption that the highest bending loads will occur in the first ¼ cycle, or in 0.063 s. In an actual deployment, the panel is expected to reach its maximum deflection after 0.063 s; then the tip will start back, driven by the restoring forces in the bent spar and the compressed cruise damper spring. At this point, the total energy absorbed by the bending of the panel and the compression of the cruise damper will equal the original kinetic energy of the panel at first contact. It was assumed that the cruise damper piston is of a maximum mass and can be accelerated from rest to the panel velocity in no more than 0.004 s.

The total kinetic energy and energy-absorption allocations to the panel and the cruise damper are given for four different deployment velocities in Fig. 14. The selected maximum deployment velocity of 0.22 rad/s provides the following characteristics:

(1) Kinetic energy of panel, 5.35 in-lb.

(2) Energy absorption allocated to panel spar bending, 2.62 in-lb.

(3) Energy absorption allocated to cruise damper, 2.73 in-lb.

In an actual deployment, the distribution of energy between the panel and the cruise damper will probably be lower than a 2.62:2.73 ratio; however, a good margin of safety is provided. For example, if the energy distribution between the panel and the cruise damper is in a 3:2 ratio, the panel spar will absorb 3.21 in.-lb or 74% of its capacity, which is based on a conservative maximum spar bending moment of 960 in.-lb. In determining the maximum moment, prestressing of the beryllium channels was included, and the channels were assumed to be originally formed to the extreme out-of-straight tolerance condition, then deflected to the straight condition during the bending of the spar. Actually, the

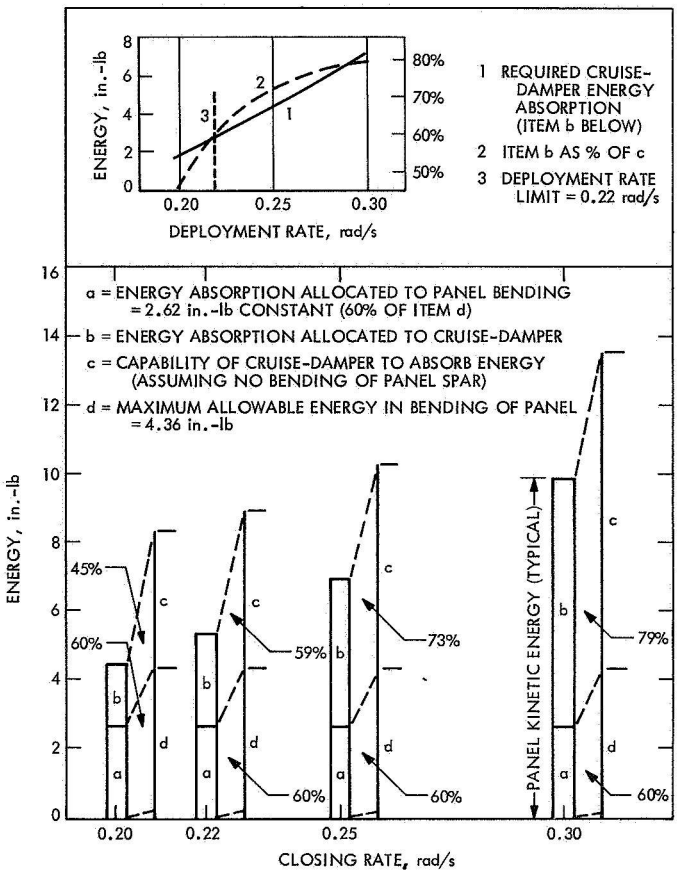

Fig. 14. Energy distribution at end of deployment

forming consistency was such that the straightness of all channels was well within tolerances.

VII. Deployment Mechanisms

An important assumption in determining deployment spring torque requirements concerns friction losses. These losses result from the friction of the bearings and spring and the resistance to deployment of the electrical wiring and the attitude control gas hoses or swivel connections. For analytical purposes, it is assumed that these losses can vary from zero to 3 in.-lb at any point throughout deployment. Based on this assumption, two types of springs have been examined: a conventional torsion spring and a Negator RW (reverse wound) constant-force spring. The conventional spring has the disadvantage of minimum torque at the end of deployment. When the friction losses and rotary damping coefficient are assumed to be maximum (the low-temperature condition), the deploying velocity is 0.044 rad/s and the net torque at closing is 1.0 in.-lb. This may not be sufficient to engage the cruise damper latch. For comparison, the constant-force spring, under the same extreme conditions, provides a deploying velocity of 0.063 rad/s with 3.0 in.-lb of torque. At the other extreme, with no damping and no friction losses, both types of springs provide about the same deployment velocity of 0.30 rad/s. For these reasons, a definition of the deployment spring has been established as follows:

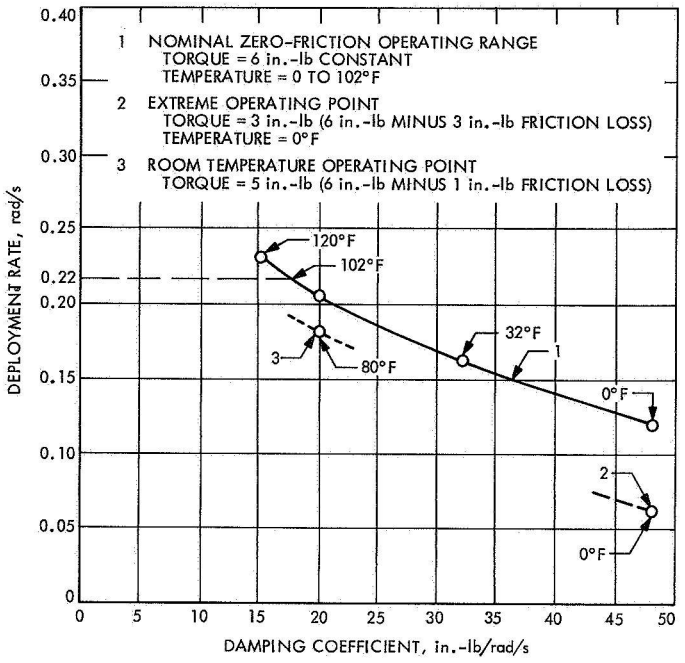

Fig. 15. Deployment rate vs damping coefficient

Spring type — Constant-force (Negator RW type).

Spring torque — 6.0 in.-lb nominal.

To determine rotary damping effects on deployment velocities, several deployment time–history curves were developed. From these time–histories, damping coefficient vs deployment rate curves were developed as shown in Fig. 15. For deployment of the lightweight solar panel, two Sesco Manufacturing, Inc., rotary dampers will provide adequate deployment velocity limitation. However, as shown in Fig. 16, these dampers are temperature-sensitive. Also, test experience has shown that these dampers behave more consistently with the regulating valve in the closed or near-closed position. Therefore, curve 1 of Fig. 16 has been selected as the centerline definition of rotary damping characteristics. (These curves were developed for Sesco Manufacturing, Inc., rotary damper part 1025-800; however, comparable dampers could be substituted.)

Curve 1 of Fig. 15 is the result of combining the centerline spring and dampers and assuming friction losses

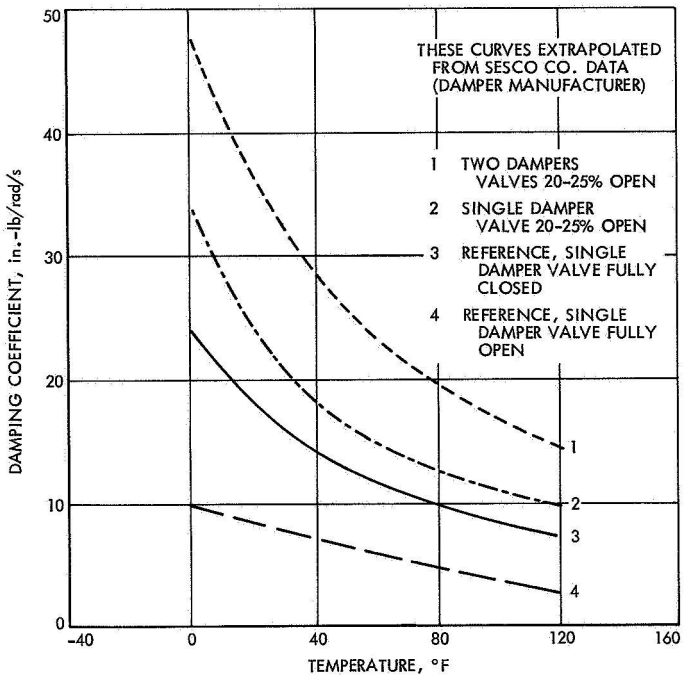

Fig. 16. Temperature effects on damping

to be zero. This curve indicates that the damper temperature should be limited to a maximum 115°F to stay within the deployment velocity limit. This can be done by shielding or thermal coating of the dampers. Controlling the minimum damper temperature may be more difficult. Point 2 of Fig. 15 shows the condition with the damper temperature of 0°F and with 3.0 in.-lb friction losses. A deploying rate of 0.063 rad/s results. The silicone oil used in the dampers allows operation at temperatures as low as −65°F. However, below 0°F, the deploying velocity may be too low to allow latching of the panel to the cruise damper. Two alternatives are possible:

(1) Insulation of the dampers to retain the latent heat at launch.

(2) Design of the latch to operate at low deployment velocities. The constant-force spring provides a minimum latching force of 0.46 lb regardless of the deploying velocity. However, the total time to deploy and latch might be several minutes.

It is felt that both insulation of the dampers and a design of the latch to operate at low deploying velocities would be desirable to assure reliability of the deployment latching.

VIII. Boost Damper Characteristics

In the launch position, the panel requires dampers to be attached to the outboard end of the main spars in a manner similar to that used for *Mariner* spacecraft solar panels. *Mariner* Venus 67 damper parts were evaluated for use in the random and sine vibration tests. The result of the initial tests showed that the effect of viscosity was much less than expected, that good repeatability was not possible, and that extrapolation toward zero amplitude was not feasible. Each damper showed anomalies in the curve shapes of damping vs amplitude. The possibility of an undesirably high static friction was indicated.

On the basis of examinations of plotted data from these tests, two "overall best" dampers were selected for use in the panel dynamic tests. Additional tests of these dampers were then made with two O-rings and 30,000-centistoke oil to reduce friction. The results of the tests on these two damper assemblies are shown by Fig. 17. The initial portion of the oscillograph records for these tests was recorded with gradually increasing force in an attempt to obtain the force at which motion began. The background electrical noise of the system was large enough to mask the initiation of motion. Extrapolation of the response curve to zero indicated that the breakaway force was at least between 1 and 2 lb. Initial friction is important because the beam will oscillate as a pin–pin beam without damper motion unless the forces at the damper exceed the "stiction" force. The importance is magnified because the actual test excites the panel only at its hinges, whereas the simulated test environment is for translation of all four panel attachment points. As a consequence, the forces at the damper are appreciably less than they would be for the translation conditions, even though the hinge excitation is increased to excite the panel modes to equivalent amplitudes. The result is that the concentrated weights at the outboard end (jet assembly and sun sensor) have minimum motion during the test excitation, but translate at the same excitation level as the hinge during the actual (specified) excitation. With no structural damping assumed, the requirement for the dampers is to provide (at least) the required generalized damping force at the amplitude for zero margins of safety. At resonance, the generalized damping force must equal the generalized driving force. The dynamic analysis of a flight panel considers excitation in translation at four points: the two hinges and the two damper locations at opposite ends of the panel. However, the random and sinusoidal vibration of the test panel is accomplished by exciting the panel only at the hinges, with the dampers attached

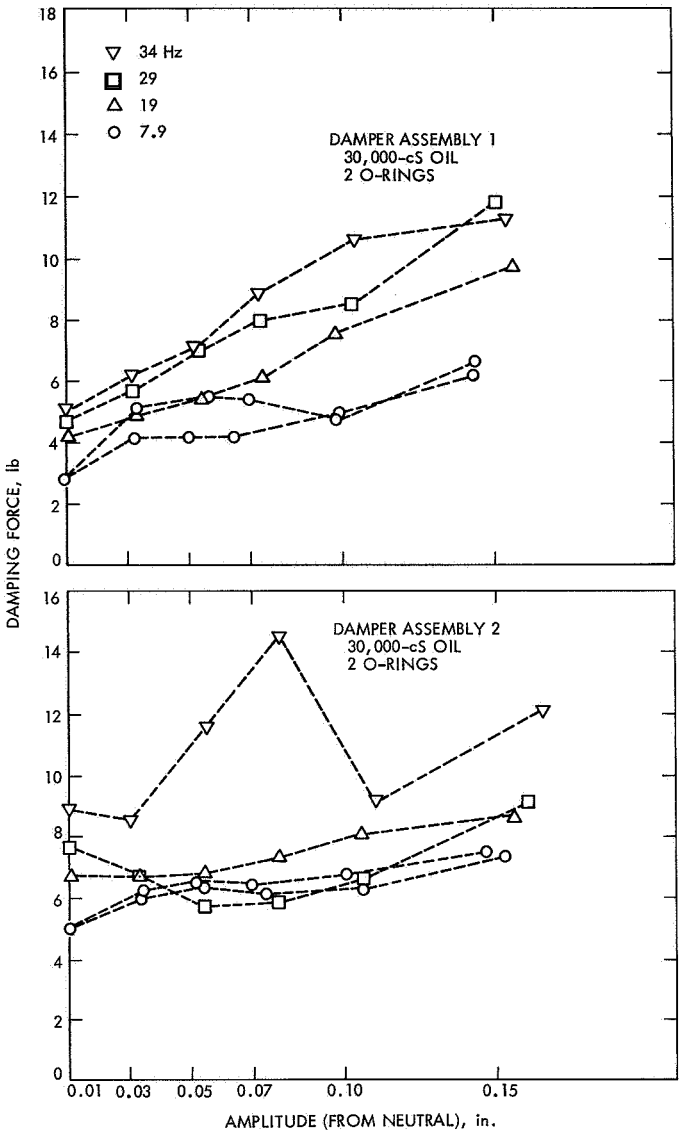

Fig. 17. Boost damper test results

to ground. The uniform translation driving forces for both of these conditions (based on a 1-g excitation) are given in Table 3. The modes underlined in this table are the three which are significantly excited below 100 Hz by the 0.707-*g* test requirement. The specified test ratio is used to determine equivalent excitations at the hinge points for the specified 0.707-*g* test excitation. The ratio for each mode is multiplied by 0.707 *g*, resulting in a range of values from 4.56 *g* for the rigid rotation mode to 0.67 *g* for the first bending mode. For the analyzed panel configuration, the generalized driving forces and the limiting amplitudes at the damper locations are given in Table 4 for the important modes. The total damping force is equal to the generalized driving force divided

Table 3. Driving forces, sinusoidal test

Mode	Driving force at 1-*g* excitation		Specification/test
	Specification (4 points), lb	Test (2 points), lb	
Rigid rotation, 7.9 Hz	13.53	2.09	6.47
First torsion, 19.2 Hz	−0.105	−0.048	2.09
First shear, 28.6 Hz	13.82[a]	2.81[a]	4.93
First bending, 34.3 Hz	4.24	4.49	0.94
Second torsion, 68.6 Hz	−0.031		
Chord bending, 81.0 Hz	−0.017	−0.065	0.25

[a]Based on excitation in the in-plane direction.

Table 4. Boost damper parameters

Mode	Generalized driving force for 0.707 *g*, lb	Amplitude at damper location (normalized)	Total damping force required (2 dampers), lb	Limiting amplitude at dampers (for zero margin of safety), in.
Rigid rotation	9.6	1.0	9.6	0.15
First shear	9.8	1.0	9.8	0.20
First bending	3.0	0.462	6.5	0.077

by the normalized modal amplitude at the damper locations.

Examination of the damping force curves (Fig. 17) shows adequate excess force over the damping force required to control the response of the panel within amplitude limits. (The damping forces shown in Fig. 20 can be doubled because two dampers are used.)

IX. Test Program

The test activities and results of the type approval test program to which the prototype test panel was subjected are diagrammed in Fig. 18. Performance was monitored throughout the environmental test program by means of 21 strain gages, 17 accelerometers, and 30 thermocouples. Location of instrumentation was determined by analysis during the design of the solar panel.

A. Modal Survey Test

The modal survey test was conducted to determine the mode shapes, frequencies, and modal damping of

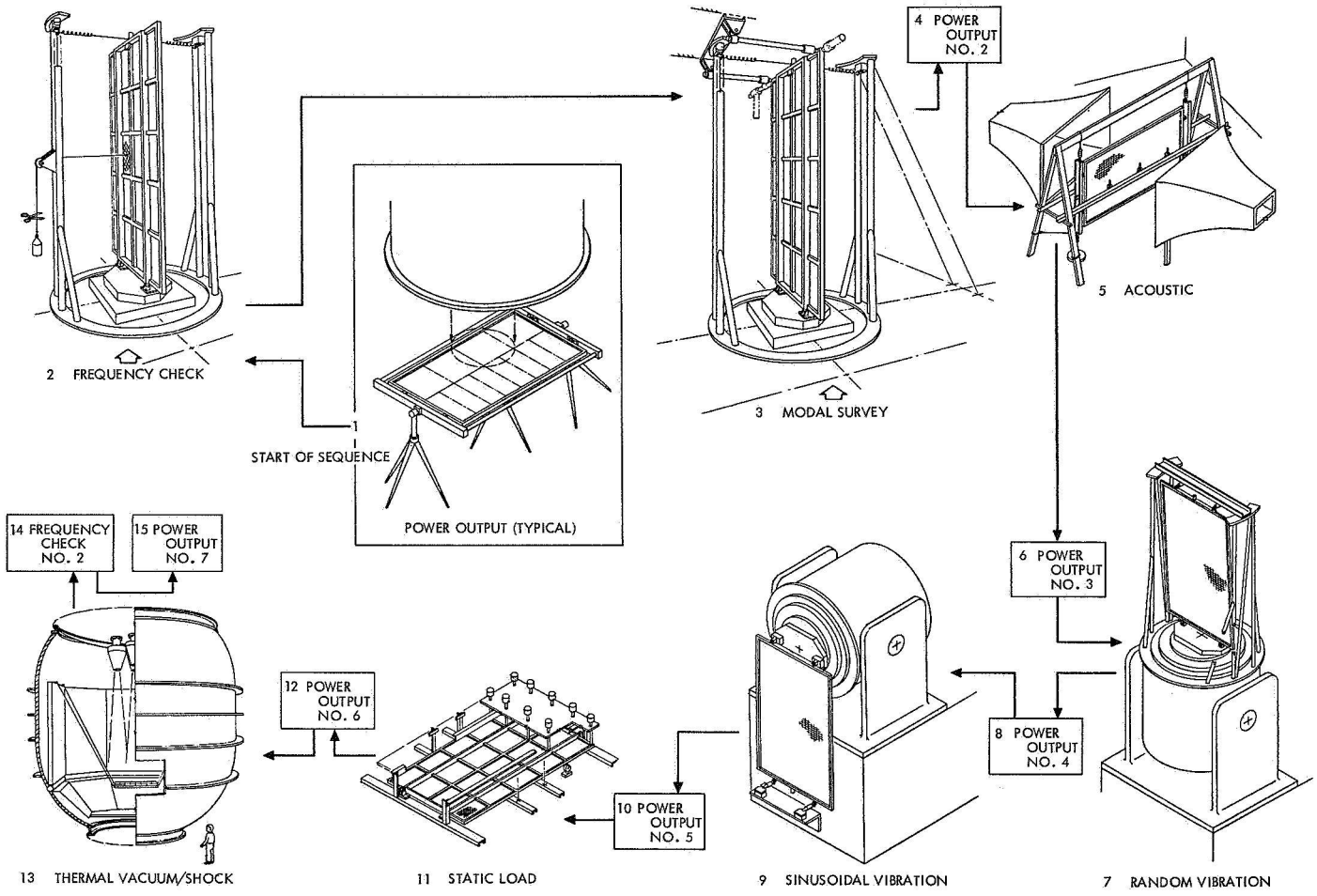

Fig. 18. Test sequence

the test panel for the resonant frequencies below 100 Hz. Before testing, analyses were made to predict the resonant frequencies and mode shapes for the test panel configuration in the pin-free condition, which was the modal test condition. Selection of instrumentation locations was based on these analyses. The panel was supported at its hinges in a floor-mounted fixture and was held in a vertical position by two pretensioned, soft springs attached to the simulated attitude control jets at the outboard center of the panel. Excitation was provided by means of small voice coils attached at two positions at the outboard end of the panel. A third set was used to excite the panel in shear (in-plane excitation). During the first sweep in the torsion mode, the amplitude increased rapidly at about 13 Hz, causing the monitoring limiter to shut down the excitation. Subsequent sweeps, with the limiter adjustment relaxed, showed that the panel torsional stiffness was less than expected. Some difficulty was encountered in the shear mode at about 24 Hz, where a sudden amplitude increase was encountered, accompanied by high-frequency content and acoustic noise. This was attributed to a free play tolerance buildup between the panel hinges and the fixture. An attempt to measure panel motion at points other than the fixed accelerometer locations was made, but the roving pickup measurements were unsatisfactory because the pickup would either influence the panel or it would bounce and not follow the panel vibration frequency. However, node positions were successfully determined by sensing no-motion points with the finger tips. The measured frequencies and a comparison with the calculated frequencies for the various modes are given in Table 5. When allowances were made in the calculations for the added instrumentation weight, the calculated results still indicated a higher stiffness than found by test for both the bending and torsion modes. The bending stiffness was about 80% of calculated; the torsion stiffness was about 65% of calculated. This was later substantiated by the static load tests.

Table 5. Modal test results

Mode	Frequency, Hz		Damping coefficient	
	Measured	Calculated[a]	XY plot	Decay
First torsion	12.2	17.0	0.038	0.035–0.038
First shear	22 (XY) 28 (decay)	27.5	NG	0.037
First bending	28.4	33.9	0.11	0.104
Second torsion	50	67.9	0.062	0.062
Chord bending	58	80.9	0.062	0.063
Large substrate	68–71		0.066–0.085	None
Small substrate	78		0.063	None
Unidentified	90±	103.0	0.045	0.033–0.036

[a]Calculated frequencies not corrected for final measured weight or for instrumentation weight.

Damping factors determined by the two methods given in Table 5 showed acceptable agreement. The minimum measured damping was equivalent to a magnification of 30 for the first torsion and shear modes. The maximum damping, for first bending, was equivalent to a magnification of 10. The mode shapes generally agreed with the calculated values for all but the highest frequency measured.

B. Acoustic Test

The acoustic test was conducted to expose the test panel to an overall acoustic noise level of 150 ±3 dB and to determine the panel response. The test panel was exposed to a reverberant acoustic noise field of 148.2 dB overall. The specific ⅓-octave band levels and tolerances were the controlling levels. The test panel was supported in the test chamber between two 80-Hz cutoff exponential horns. Two separate systems controlled the Altec-Lansing acoustic transducers driving the horns to ensure random excitation of the panel. Microphones mounted adjacent to each side of the panel were used to measure the environment. The only visual indication of motion during the test was a blurring of the exposed substrate tapes, visible as a white line between the solar cell modules. The panel structure response was nominal; however, the substrate response was four times greater than estimated. The measured response in the largest substrate bay indicated a response of 305 g rms. This may have been due in part to the upward shift of the substrate resonant frequencies (from about 35 to 60 or 70 Hz for the fundamental mode). Despite the high accelerations, no separation of the cells from the substrate occurred, and the allowable stress for the RTV-40 cell bonding agent was not exceeded. The highest strain was measured on a main spar near the middle of the panel, with an equivalent maximum 3-sigma stress of 4300 lb/in.^{2}. No structural damage was observed as a consequence of this excitation.

C. Random Vibration Test

The random vibration test excitation input was along the launch vehicle roll axis, which is nearly parallel to the plane of the panel in the stowed position. Because of the small component of random excitation normal to the panel and the dampers attached at the tips, important dynamic response was not expected. The only area of concern was the possible effects of the concentration of mass due to the attitude control jet simulation and the sun sensor simulation. For this area, an acceleration limiter setting of 40 g peak was calculated for the initial test runs. An adapter fixture attached to a Ling 249 vibrator supported the test panel at its hinges. The panel was tilted 4 deg off the vertical axis of the vibrator and supported at the tip by two dampers. Prior to panel installation, evaluation of the test fixture was made to obtain the desired random vibration spectrum at both hinge points on the fixture. The required spectrum and the measured input spectrum used in this test are shown superimposed in Fig. 19. Stress and acceleration levels were low in the random vibration test, as expected. The area of most concern, the responses and stresses near the simulated equipment at the panel tip, did not show excessive response levels. The longitudinal response in this area was 6.1 g rms. A value of 8.05 g rms normal to the panel was obtained from accelerometer A10 on the longitudinal intercostal.

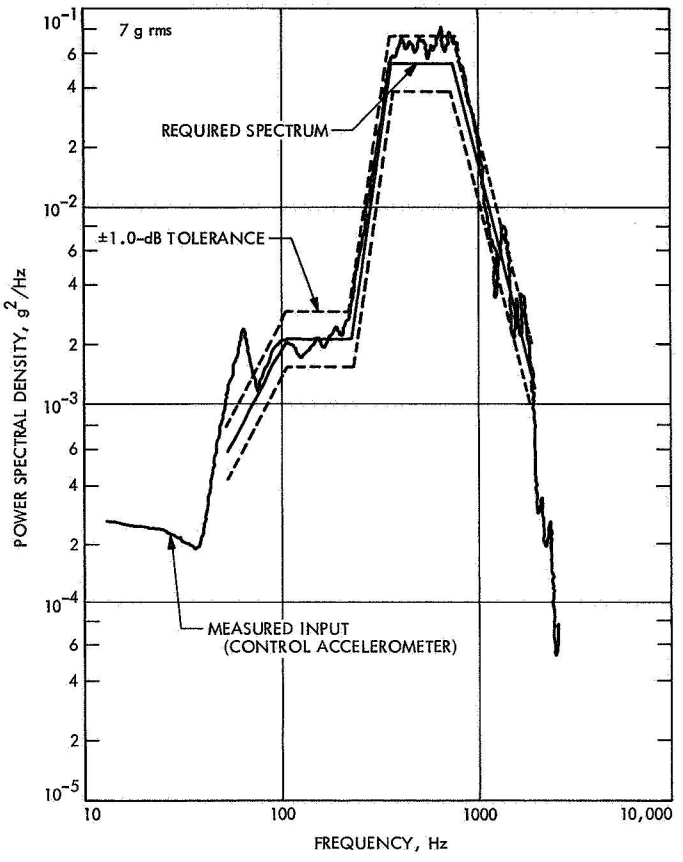

Fig. 19. Random vibration test spectrum

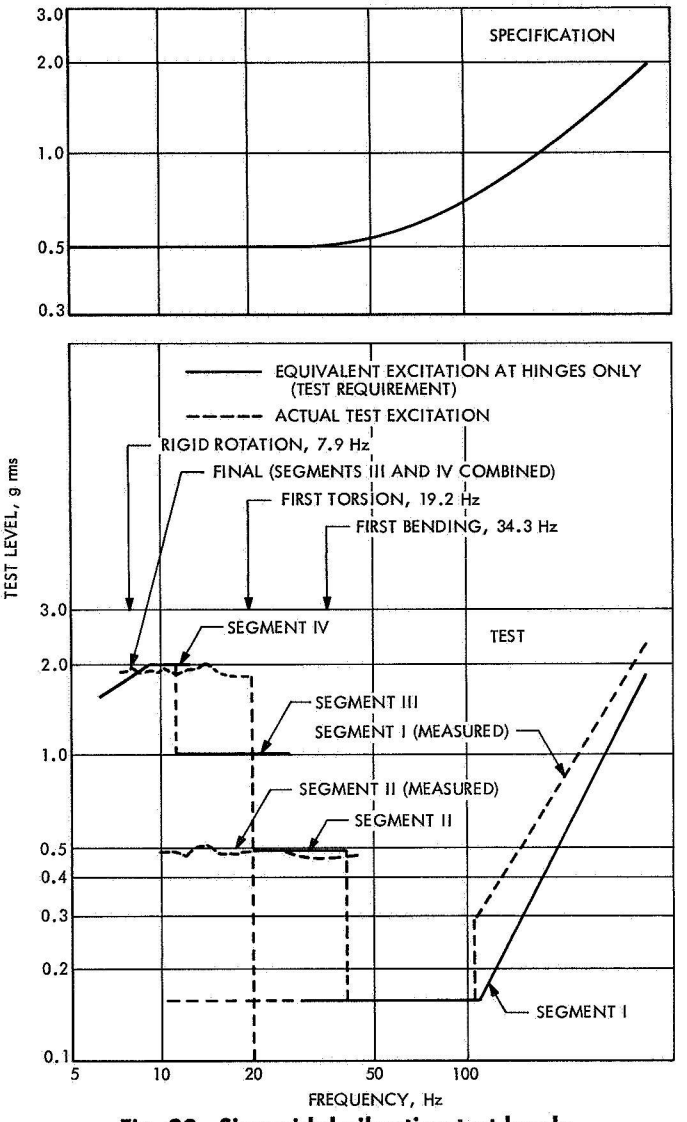

Fig. 20. Sinusoidal vibration test levels

The large substrate exhibited 14.6 *g* rms. The general level of 3-sigma peak stress was about 600 lb/in.², with a maximum value of 1100 lb/in.² in the main spar cap near the hinge. No structural damage was observed as a result of this test. Damage to a silver mesh interconnector, possibly attributable to this test, was subsequently found.

D. Sinusoidal Vibration Test

The sinusoidal vibration test was designed to provide excitation of the panel at the hinge points that would produce response of the panel to the levels equivalent to the response when excited to the specified levels at the four spacecraft attach points. To simulate the specification requirements, the panel required excitation in translation normal to the panel at four points, the two hinges and the two tip fittings. In order to avoid the use of two vibrators, the test panel was excited at the hinges only, with the panel tip supported by dampers. The sinusoidal vibration test was conducted in four steps to obtain responses equivalent to the specified condition. The test panel was suspended by the hinges from an adapter fixture attached to the Ling 249 vibrator as shown in Fig. 18. Test levels are shown in Fig. 20. The upper chart in this figure shows the specification levels for four-point excitation. Planned and actual test levels are superimposed in the lower chart. The planned levels were achieved in four test segments, selection of which was based on the predictions of important modes and frequencies and on the limitations of the test equipment. The test was accomplished in segments to obtain "equivalent" excitation, which varies with each resonant mode. A problem arises when resonances are close and the higher frequency modes require a significantly lower excitation level. Under these circumstances the excitation at the lower frequency mode can overdrive the higher frequency mode.

The test spectrum calculated for the test procedure from the analytic solutions for resonant frequencies required revision to account for the resonances measured in the modal test. The analytic calculations had indicated only very low excitation forces for the first and second torsion and for the chord bending modes. This results from the stiffness symmetry and only a small amount of mass dissymmetry about the longitudinal axis. Thus the critical motions for the panel for this test were expected to be the response at about 8 Hz of the rigid rotation mode and the response at the first bending mode. The tip damper requirement for the 8-Hz mode was to limit the travel of the dampers to something less than 0.15 in. in order to ensure that the damper force would increase with amplitude. For the bending mode, the requirement was to limit the bending stresses. Stress measurements show that the "rigid rotation" stresses are about 15% higher than the bending mode stresses. Examination of the stress and acceleration traces show a large component of a higher frequency which is apparently driven off-resonance by the nonlinear characteristics of the damper. The highest stress measured in the main spar caps was 3250 lb/in.^{2}, as compared to 10,900 lb/in.^{2} for zero margin of safety. In the main beam channels the maximum stress was 1240 lb/in.^{2} for zero margin of safety. The nonlinear characteristics (probably due to the dampers) were seen in the oscillograph record for the starting portion of the final test sequence. The traces had the high-frequency content filtered out, but an appreciable, almost harmonic, content remained. At this frequency and amplitude, the ratio of damping forces between the two dampers is about 1.5. Peak stresses from the combined components are 3250 lb/in.^{2} as compared to 2860 lb/in.^{2} for the bending mode condition. Measured stress levels were generally related to each other by ratios similar to those for the calculated zero-margin-of-safety stresses. With one exception, the accelerations experienced during the segment I sweep were less than 5 g on the structure even at high frequencies. For accelerometer A10, on the longitudinal intercostal, one sharp spike reached 15 g. The substrate response had peak values of 8 and 12.5 g on the large and small substrate bay, respectively. The strain gages showed their peak values at the 20-Hz bending frequency. No structural damage was encountered in this test. However, another silver mesh pigtail failure was discovered in the subsequent power output check.

E. Static Load Tests

The static load tests demonstrated greater panel flexibility than anticipated. The two specified loading conditions were: (1) 8-g distributed load normal to the panel and, (2) 50-lb point loading. In the 8-g, or bending test, the panel was supported at the hinges and the tip latch pins (two points at each end) and loaded by weights applied at the structural intersections. In the 50-lb, or torsion test, the panel was supported at the two hinges and at one tip latch pin. The load was applied at the other tip latch pin. In both cases deflections were measured with dial gages and stresses with strain gages. The panel was loaded to 100% of the planned test load in both the bending and torsion condition. As the load was applied in increments, deflections higher than initially predicted were noted. Increased flexibility was expected because of the lower stiffness indicated by the modal survey. However, as the test weight was increased from zero to 100%, the deflections remained linear and the strain gage readings indicated that stresses were not excessive. The torsional condition was of the greatest concern. In this condition, a loading in excess of 40 lb was sustained for 40 min without damage or permanent set to the panel cell. The deflections, plotted at the measurement station, for the bending and torsion tests are shown by Figs. 21 and 22, respectively. Measured stresses did not exceed allowable limits. Bending deflections at the middle of the panel exceeded the calculated values. This reduction in stiffness is validated by the results of the modal test. When adjustments of the calculated frequencies are made for the added instrumentation weight and the measured weight of the panel, the calculated stiffness approximated the stiffness required to produce the measured deflections.

F. Thermal–Vacuum–Shock Tests

The thermal–vacuum–shock tests were conducted to obtain voltage–current data at earth and Mars intensities, to determine operating parameters of the zener diodes, and to demonstrate the structural integrity of the array under "type approval" levels. The test panel was exposed to a range of temperature and solar simulator intensities while in a vacuum of 10^{-5} torr. A history of the actual test sequence and conditions is given in Fig. 23. No structural or electrical degradation of the test panel occurred as a result of the thermal–vacuum–shock tests. Voltage–current and temperature data obtained substantiated the analytical predictions of the thermal and electrical performance of a flight configuration panel of the lightweight solar panel design. An important characteristic of this design that was demonstrated was the lower operating temperature compared to more conventional substrates. At 140 mW/cm^2 simulated solar intensity, the operating temperature was

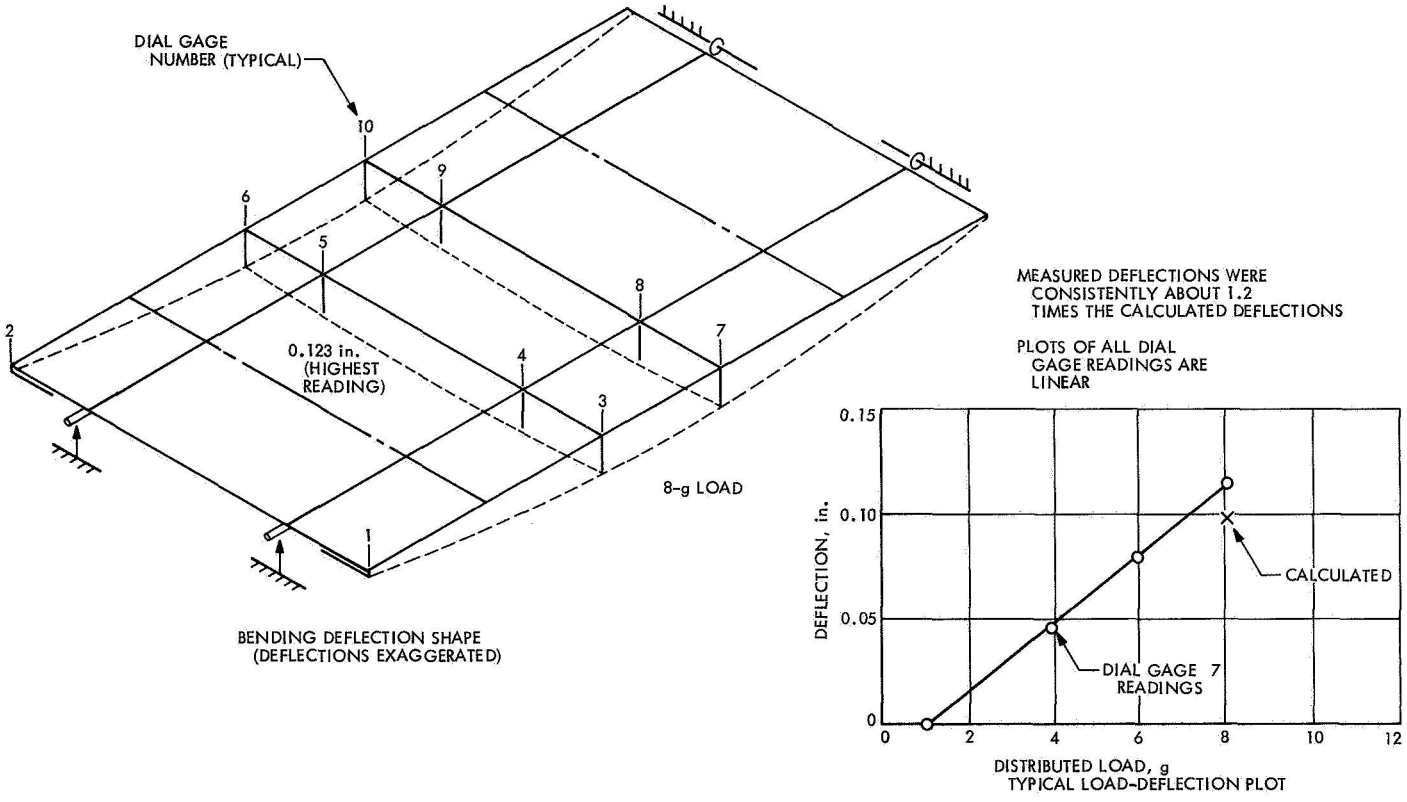

Fig. 21. Deflections — 8 g load

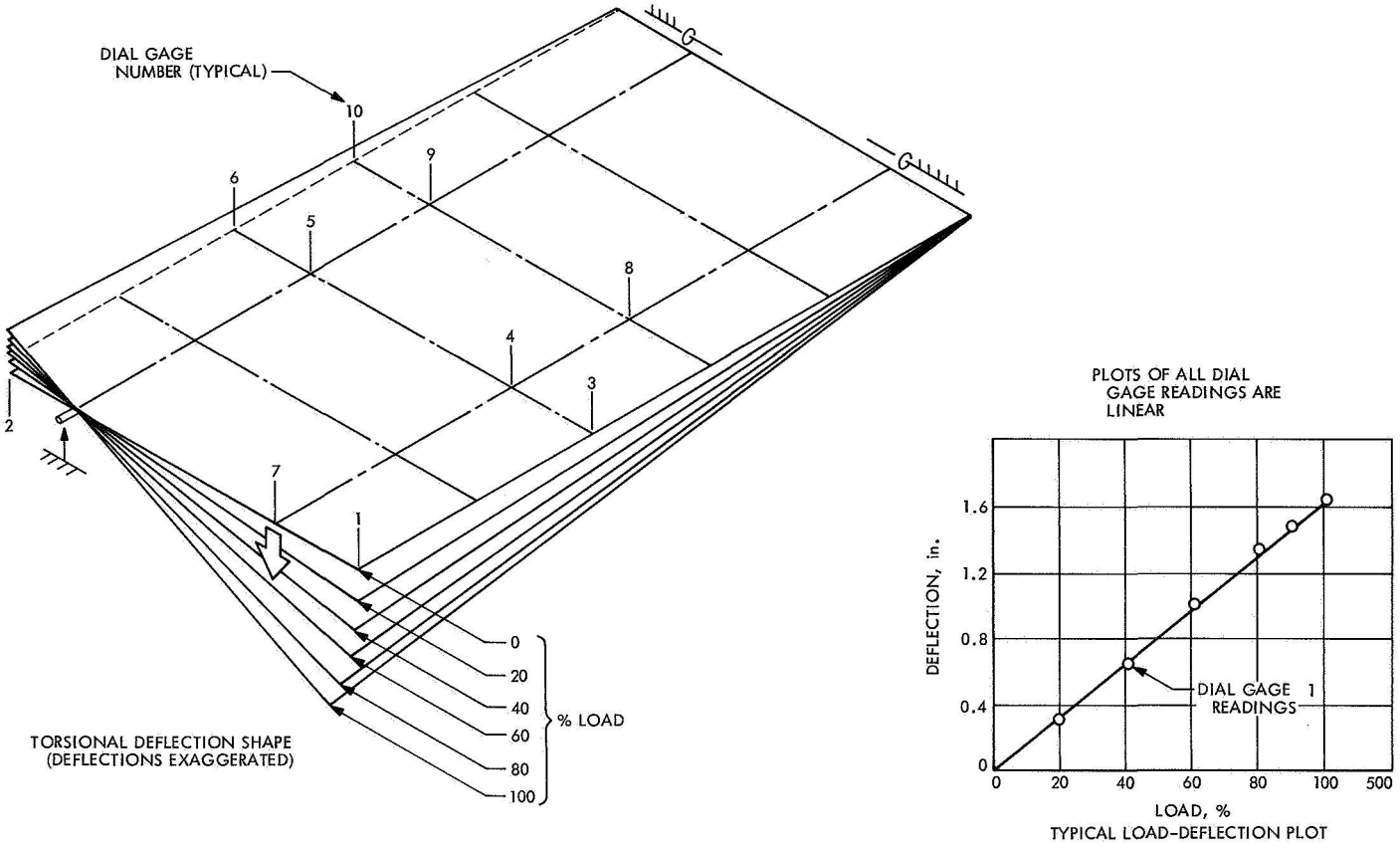

Fig. 22. Deflections — 50-lb load

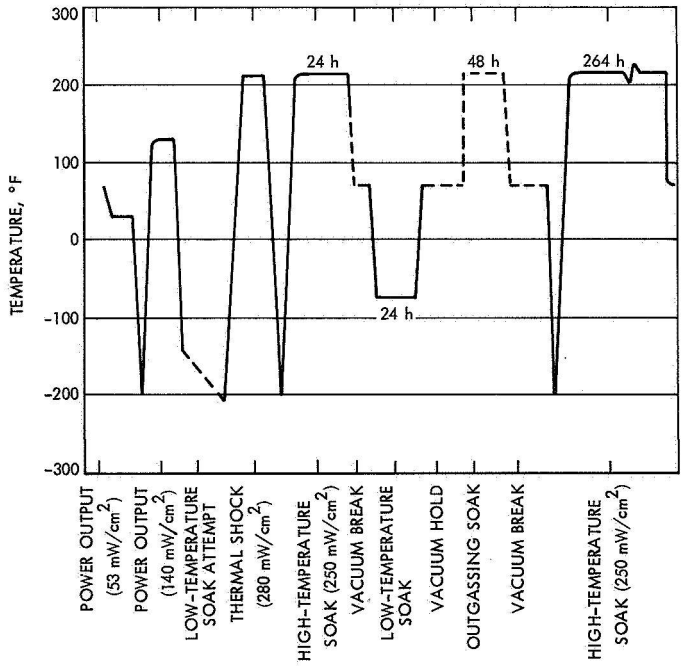

Fig. 23. Thermal–vacuum–shock test history

48.5°C compared to approximately 55°C nominally predicted for the *Mariner* type of substrate. The open substrate design also exhibits a short solar cell warmup time. This is important because of the short time that the zener diodes operate during the thermal up-shock. The shorter operating time indicates that a less severe derating factor can be used, resulting in fewer zener diodes required and a lower weight penalty. During the final period of high temperature soak, power to one solar lamp was unintentionally interrupted for a period of 15 min, resulting in a 109°C temperature differential on the panel; no damage resulted. Therefore, the ability of this array to withstand wide temperature differentials was also demonstrated.

G. Substrate Frequency Tests

The substrate frequency checks were performed once at the start and once at the completion of the series of environmental tests. A comparison of the results of the two checks was used to determine if any significant relaxation in the tension of the fiberglass substrate tapes had occurred. The measured substrate frequencies, before and after the environmental tests, are shown below:

	Pretest frequency, Hz	Posttest frequency, Hz
Large substrate bay	74	69
Small substrate bay	78	74

The fundamental frequency dropped 4–5 Hz during the test series. The test most likely to cause a relaxation of the substrate tension was thermal–vacuum–shock; this test included a thermal soak of 212°F (100°C) for 12 days under vacuum. The 6% drop in frequency represents a small amount of relaxation of substrate tension and does not significantly affect panel performance.

X. Damage Incurred During Test

A. Silver Mesh Pigtail Design

The silver mesh pigtail design has been found to be vulnerable to damage during subassembly, installation, and testing. These pigtails are about 1 in. long by ⅛ in. wide when folded double from the original ¼-in. width, and protrude from the extreme corners of each submodule assembly. They are subject to bending over the solar cell edges, either during handling of the submodule or during bonding, where vacuum bag pressure is applied. During vibration testing, a flexing of the pigtails occurred owing to the motion of the cells and substrate relative to the structure and buses.

The failures that occurred during the test program were not evident in a visual examination but were detected by electrical continuity checks. In all six cases, the breaks in the silver mesh were hidden by the RTV-40 thermal control coating, which also held the broken mesh together. When a suspected pigtail was probed, continuity would be broken and sometimes the pigtail would separate physically. The breakage during testing could not be attributed to any one test because of the difficulty of detection. However, the first failure was noted at the time of the power output test following the acoustic test. Subsequent failures were noted after the random vibration test and during the thermal–vacuum test. The failures occurred only at the positive-to-bus and submodule-to-submodule connections.

B. Mechanical Damage of Solar Cells and Coverglasses

Mechanical damage of solar cells and coverglasses occurred twice during testing. The first instance was discovered at the time of the setup for the acoustic test. Two cell assemblies adjacent to the inboard, or hinge, edge of the panel were broken. The appearance of the fracture and the proximity of finger marks on the structure indicated that these cells were cracked by finger pressure during handling.

The second instance occurred during the static load test. As the loading was increased, the dial gage probe at the unsupported outboard corner of the panel slipped off of the slanting structural surface and contacted the extreme corner cell, causing the breakage. Edge cracks were found in both cells and coverglasses. Generally, these cracks were barely discernible, hairline cracks extending about ⅛ in. from the edge of the cell or, in some cases, running diagonally across a cell corner. Triangular chips at the edges were also noted on some cells. No electrical degradation has been attributed to this cell breakage. Of the 36 cells and 55 coverglasses that were cracked, 13 cells and 18 coverglasses were found to be cracked at the start of the test program. The total quantity of cells on the panel was 6480.

Cell and coverglass damage was generally distributed over the panel and throughout the test program as shown in Table 6.

Table 6. Solar cell/coverglass damage

Phase	Solar cells	Coverglass
Initial inspection	13	18
After modal survey	8	5
After acoustic test	1	1
After random test	5	9
After sinusoidal test	2	5
After static test	4	10
Final inspection	3	7
Total	36	55

XI. Fabrication Details

A. Beryllium Sheet Material

Beryllium sheet material was purchased in the widths required for forming channels or in net widths for flat parts. Forming was done in a stainless steel die. The die was heated and the forming done in a hot platen press with ceramic platens on the top and bottom. Both die and part were heated to 1375°F (746°C); the part was then "creep formed" by lowering the upper platen at 0.1 to 0.2 in./min until the die stops were reached.

The channel straightness required by the design was 0.002 in. in 10-in., and the channel flange perpendicularity requirement was 0.005 in. To produce channels to the required straightness, fluid pressure was applied vertically by means of a stainless steel bladder to force the die and hence the channel to conform to the flat-bottom press platen. Fluid pressure was applied horizontally by means of an expanding stainless steel tube to force the channel flanges to conform to the perpendicular sides of the punch and the straight fixed side bar of the die. A pressure of 6–8 psi was applied to the upper bladder for 2 min, then reduced to zero. A pressure of 200 psi was applied to the steel side tube and the 6–8 psi reapplied to the upper bladder for 10–20 min. The upper platen was then raised slightly to take the platen weight, but not the upper bladder pressure, off the part; then the part and die were cooled to 800°F (426°C) from 1375°F (746°C) and removed from the pressure. At 500°F (260°C), the part was removed from the die, inspected and trimmed. Excess flange height was removed by cutting with an abrasive wheel. Channels were inspected by penetrant for defects, followed by chem-milling. Chem-milling and cleaning were done using an ammonium bifluoride/phosphoric acid solution and a de-smut solution of sulfuric/chromic/phosphoric acid solution.

B. Titanium and Steel Parts

Titanium and steel parts were cut from sheets for gussets, clips fillers, etc. Titanium hinge fittings, tip latch fittings, and cruise damper fittings were machined from solid plate stock, then finished by electrical discharge machining using a graphite electrode.

C. Structural Member Subassemblies

Structural member subassemblies, or "sticks," consist of two channels adhesive-bonded with cap strips over the length of each channel joint. Heat-resistant Mylar adhesive tape was used to hold parts in proper relation to each other when the "sticks" were placed into the bonding fixture. Heat for bonding was supplied by an electric blanket under the baseplate of the tool, and pressure was applied from line pressure through a regulator to an air bladder on the tool. The sticks were bonded by heating to a temperature range of 225°F (97°C) to 250°F (110°C) with a pressure of 17–100 psi. The assembly was maintained at that temperature and pressure for 1 h. After bonding, the "sticks" were cut to length and miter-cut as required.

D. Sun-Side and Dark-Side Frames

Sun side and dark side frames were made by similar processes. Details to be bonded were cleaned, adhesive was placed on one face of each mating surface, and tubular members, gussets, and clips were jig-located on the bonding platen. Rubber pads were placed on top of gussets and spring pressure plate setups were placed over each gusset and adjusted to give the required vertical bond pressure. Rubber-faced, calibrated, spring-located clamps were placed to apply horizontal pressure to clips previously taped in place at the inside and outside of each corner joint. An aluminum frame was placed over the structure to be bonded and covered with a nylon cover and aluminum foil insulation blanket. Warm air was blown inside the tent-type enclosure; this arrangement prevented major temperature variations, and the temperature was maintained within ±5°F. The major source of heat was derived from heating blankets under the jig base; bonding took place at a temperature of 225°F (101°C) to 250°F (121°C) for 1 h.

E. Fiberglass Tape Substrate

The fiberglass tape substrate was bonded on the same hot platen table used to bond the sun-side and dark-side frames. The fiberglass tapes, preimpregnated with epoxy

resin in the uncured stage, were laid and spaced in a tension bar frame to hold the tape ends. Tapes were tensioned by hand and held in place with double-backed adhesive tape at the tension bar. The tapes were then covered with a Teflon parting film, and a nylon vacuum bag was sealed to the outer edges of the jig baseplate. A 10-in. minimum vacuum was drawn, and the jig baseplate was heated to 300°F (149°C). The assembly was then cured for 30 min at 300°F (149°C) and for 4 h at 350°F (177°C). After the curing, the assembly was cooled to 150°F (65°C), the vacuum bag and Teflon parting films were removed and the substrate assembly was visually inspected and node bonds were checked.

F. Structure Final Assembly

Final assembly of the structure, consisting of sun-side/fiberglass tape substrate/dark-side, is adhesive-bonded using the same heated platen, spring clamp fixture used to assemble the individual components. Adhesive was applied to the sun-side frame, which was then set on the bonding platen, adhesive side up. The substrate, still in its tension frame, was properly oriented onto the sun-side frame. The substrate was tensioned to 12 lb per linear inch of edge by built-in adjustments. After this was done the dark side frame was coated with adhesive as required, and placed on the sun-side/substrate assembly. After alignment, pressure was applied and final bonding performed. Curing was done using the same temperature fixturing as required to bond the sun-side/dark-side frames. Figures 24 and 25 show the completed structural frame assembly and the hinge, cruise damper, and tip fitting installations.

G. Solar Cell Assemblies

Solar cell assemblies were fabricated with 0.003-in.^{2}-thick coverglasses and 0.008-in.-thick solar cells, adhesive-bonded together with RTV 602. A bond thickness of 0.001 in. was considered necessary for minimum weight without compromise of bond strength and for uniformity. This was accomplished by weighting each cell/coverglass combination 10 min after adhesive bonding and allowing this weight to remain during the 12-h cure at room temperature. Cleaning was not done until 36 h had elapsed. Individual cell/coverglass combinations were electrically interconnected with expanded silver mesh, formed to provide a stress loop between cells. Solder cream was applied by stencil to three places on each solar cell. The interconnect was positioned over the solder cream locations and pulse-soldered. Cells were assembled into a series-parallel arrangement for adhesive bonding to the fiberglass substrate as modules.

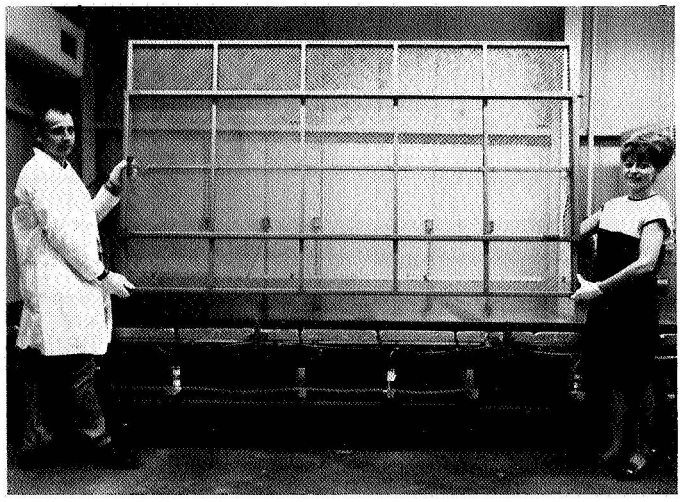

Fig. 24. Completed structural frame assembly

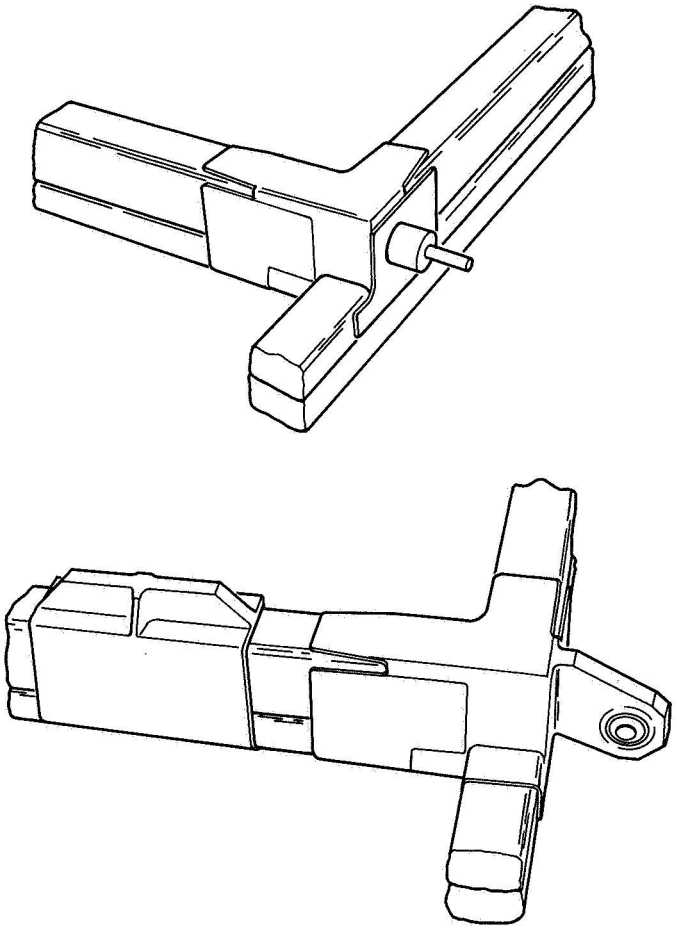

Fig. 25. Titanium hinge, cruise damper, and tip fitting installation

XII. Test Panel Final Assembly

The solar cell modules were bonded to the substrate with RTV-40. Primer was used on both the substrate and solar cell surfaces to be bonded. Adhesive was first sprayed onto the solar cell modules and allowed to partially cure. Just before the modules were bonded to the substrate, adhesive was applied to the substrate with a urethane foam paint roller. The structural assembly was set on the bonding platen and the solar cell modules laid in place. By means of fixturing and a vacuum bag system to supply uniform pressure during curing, bonding was performed at approximately 1 lb/in.^{2} for 6 h at room temperature.

After the bonding, the appropriate electrical connections were made and other hardware installed. Other hardware included such items as zener diodes and mounting brackets, blocking diodes, bus bars, and wiring. RTV-40 thermal control coating was applied by spray to specified dark-side areas and dried for 4 h at 125°F (47°C). The panel was cleaned, inspected, and made available for testing to the type approval tests discussed above.

XIII. Conclusions

The conclusions reached during the design, fabrication, and testing of the lightweight solar panel are summarized as follows. Power output measured from the five electrically connected modules averaged 24.4 W each over the five measurements made during the test program. The highest measured power was 25.2 W; the lowest measured power was 23.3 W. The pattern of power output variation indicated no measurable degradation resulting from the test program. The predicted power based on individual cell measurements at the start of module fabrication was 23.0 W per module. A design goal of 20 W/lb of specific power output has been achieved. The power output of a flight configuration panel, using 10.5% efficient solar cells as opposed to a 9.6% efficient cell specified for this development, would produce a panel having a power-to-weight capability of 23.0 W/lb. This flight configuration with the weight of three zener diodes per solar cell module added to the basic panel weight produces 20.3 W/lb. The solar panel design can accommodate a 40% increase in the weight of supported equipment, from 8.00 to 11.22 lb, with only a 3.3% decrease in specific power output. Redesign of the submodule power-out pigtails for the power transfer to the electrical buses is required. Silver mesh for this purpose is easily damaged in handling and during environmental test.

Experience during the manufacturing process has pointed out the practicality of the design. No significant problems were encountered. Some modification of the spring pressure plates is advisable for production bonding. The present process is economical but has the potential of damaging the assembly.

Test results have indicated a small reduction of the fiberglass substrate tension (6% drop in fundamental frequency) when exposed to 100°C for 12 days or extreme temperature changes at rates as high as 149°C/min for short time intervals. The solar panel and solar cell module functions are not damaged or degraded by temperatures of −100°C for 24 h, +100°C for 288 h, or when exposed to thermal down-shock rates of 107°C/min for 1 min.

First resonant frequencies of the solar panel assembly, in the pin-free condition, in bending, shear, and torsion are 28.4, 22, and 12.2 Hz, respectively. A wideband random vibration spectrum at an input acceleration of 6.9 g rms for 1 min will not result in damage to the structure or solar cells. When exposed to an acoustic field of 148.2 dB for 1 min, the solar panel will not experience structural damage. The solar panel structure is adequate to withstand an 8-g static load normal to the panel and a 50-lb load applied at one tip latch pin with supports at the other three attach points.

The basic lightweight solar panel design has met the requirements specified in the applicable test documents and conditions defined by the terms of NASA/JPL Contract 952571 and is considered to be suitable for flight hardware on interplanetary missions.

Glossary

Basic panel a flight configuration panel, consisting only of the cell stack, structure, substrate, and zener diodes, which is used for power output determination. No additional equipment or mechanisms are included

Blocking diode a solid-state component which allows current to flow in a selected direction and prevents current from flowing in the reverse direction

Cap strip one of the beryllium sheet parts comprising a structural member or "stick" (see definition herein)

Cell stack an assembly of one solar cell and one coverglass, bonded together with an RTV silicone compound

Coverglass the protective cover bonded to the solar cell

Dark side the panel surface away from the sun

Factor of safety the ratio of the ultimate design load to the limit design load

Fitting factor an additional multiplicative factor applied to fittings to account for stress complexities and concentrations

Generalized mass the "effective" mass associated with a vibration shape

Interconnectors expanded silver mesh strips which connect both parallel groups and series assemblies of solar cells

Margin of safety a positive margin of safety defined as:

$$MS = \left[\frac{\text{allowable load (or allowable stress)}}{\text{design load (or design stress)}}\right] - 1 > 0$$

Module a group of solar cells connected in series/parallel which produces system voltage and current

Node a point of no motion used in describing vibration mode shapes

Pin-free a panel support condition in which the panel hinges are supported by pins which constrain the panel against translation but allow rotation and in which the tip is supported by dampers

Pin-pin a condition in which the panel is supported at the hinges and tip in a manner constraining the panel against translation but allowing rotation

Power buses flat copper electrical conductors which collect the output of each module for transmission to the spacecraft loads

Glossary (contd)

Solar cell assembly	same as cell stack
Solar cell group	six or seven cells electrically connected in parallel by soldering each cell to a common silver mesh interconnector
Solar cell module	two or four submodules joined together in series after submodules have been bonded to the substrate
Solar cell submodule	20 or 40 solar cell groups joined together in series after submodules have been bonded to the substrate
Stick	a beryllium structural member of rectangular cross section consisting of two formed channels connected across the facing flanges by a shear web on the substrate side and a cap strip on the opposite side
Structural node	a point assumed on the panel structure for analytical purposes, usually at the intersection of structural members
Substrate	an assembly of epoxy-impregnated fiberglass tapes bonded in a grid pattern and positioned at 45 deg to the panel structural members. The solar cells are bonded to the substrate, each cell being located on a tape intersection point

NASA — JPL — Coml., L.A., Calif.

N71-20121

TECHNICAL REPORT STANDARD TITLE PAGE

1. Report No. 32-1519	2. Government Accession No.	3. Recipient's Catalog No.
4. Title and Subtitle LIGHTWEIGHT SOLAR PANEL DEVELOPMENT		5. Report Date March 15, 1971 6. Performing Organization Code
7. Author(s) Walter A. Hasbach		8. Performing Organization Report No.
9. Performing Organization Name and Address JET PROPULSION LABORATORY California Institute of Technology 4800 Oak Grove Drive Pasadena, California 91103		10. Work Unit No. 11. Contract or Grant No. NAS 7-100 13. Type of Report and Period Covered Technical Report
12. Sponsoring Agency Name and Address NATIONAL AERONAUTICS AND SPACE ADMINISTRATION Washington, D.C. 20546		14. Sponsoring Agency Code

15. Supplementary Notes

16. Abstract

This report describes the work performed by the Boeing Co., Aerospace Group, Space Division, Seattle, Washington, between July 1, 1969, and July 1970, on the Lightweight Solar Panel Development Program under Jet Propulsion Laboratory Contract 952571. The report contains technical information concerning the preliminary design, analysis, test article design, fabrication, and test of a light-weight solar panel made of a built-up beryllium structure with an active cell area of 29 ft.^{2} Evaluations are presented of the results of the modal survey, reverberant acoustic, random vibration, sinusoidal vibration, static load, thermal-vacuum-shock, substrate frequency, and power output tests.

17. Key Words (Selected by Author(s))	18. Distribution Statement
Interplanetary Spacecraft, Advanced Planetary Spacecraft, Advanced Power Sources	Unclassified -- Unlimited

19. Security Classif. (of this report)	20. Security Classif. (of this page)	21. No. of Pages	22. Price
Unclassified	Unclassified	29	

HOW TO FILL OUT THE TECHNICAL REPORT STANDARD TITLE PAGE

Make items 1, 4, 5, 9, 12, and 13 agree with the corresponding information on the report cover. Use all capital letters for title (item 4). Leave items 2, 6; and 14 blank. Complete the remaining items as follows:

3. Recipient's Catalog No. Reserved for use by report recipients.

7. Author(s). Include corresponding information from the report cover. In addition, list the affiliation of an author if it differs from that of the performing organization.

8. Performing Organization Report No. Insert if performing organization wishes to assign this number.

10. Work Unit No. Use the agency-wide code (for example, 923-50-10-06-72), which uniquely identifies the work unit under which the work was authorized. Non-NASA performing organizations will leave this blank.

11. Insert the number of the contract or grant under which the report was prepared.

15. Supplementary Notes. Enter information not included elsewhere but useful, such as: Prepared in cooperation with... Translation of (or by)... Presented at conference of... To be published in...

16. Abstract. Include a brief (not to exceed 200 words) factual summary of the most significant information contained in the report. If possible, the abstract of a classified report should be unclassified. If the report contains a significant bibliography or literature survey, mention it here.

17. Key Words. Insert terms or short phrases selected by the author that identify the principal subjects covered in the report, and that are sufficiently specific and precise to be used for cataloging.

18. Distribution Statement. Enter one of the authorized statements used to denote releasability to the public or a limitation on dissemination for reasons other than security of defense information. Authorized statements are "Unclassified—Unlimited," "U. S. Government and Contractors only," "U. S. Government Agencies only," and "NASA and NASA Contractors only."

19. Security Classification (of report). NOTE: Reports carrying a security classification will require additional markings giving security and downgrading information as specified by the Security Requirements Checklist and the DoD Industrial Security Manual (DoD 5220.22-M).

20. Security Classification (of this page). NOTE: Because this page may be used in preparing announcements, bibliographies, and data banks, it should be unclassified if possible. If a classification is required, indicate separately the classification of the title and the abstract by following these items with either "(U)" for unclassified, or "(C)" or "(S)" as applicable for classified items.

21. No. of Pages. Insert the number of pages.

22. Price. Insert the price set by the Clearinghouse for Federal Scientific and Technical Information or the Government Printing Office, if known.